Electronic Supporting Information

for

Thermally Responsive Magnetic Bistability Through Solid-Liquid Phase Transitions in Alkylthio-Functionalized Dithiadiazolyl Radicals

Juho M. Toivola, [a] Ankita Naik, [a] Manu Lahtinen, [a] Oriol Gonzàlez-Prats, [a] Andrea Perez Prieto, [a] Itziar Oyarzabal, [*b,c] and Aaron Mailman [*a]

[a] University of Jyväskylä, Department of Chemistry, NanoScience Centre, P.O. Box 35, FI-40014, Jyväskylä, Finland

[b] BCMaterials, Basque Center for Materials, Applications and Nanostructures, UPV/EHU Science Park, ES-48940, Leioa, Spain

[c] IKERBASQUE, Basque Foundation for Science, ES-48009, Bilbao, Spain

E-mail:aaron.m.mailman@jyu.fi, aaronmailman@gmail.com, itziar.oyarzabal@bcmaterials.net

TABLE OF CONTENTS

1 Experimental Methods and Details

All manipulations were performed under an atmosphere of dry argon using standard Schlenk and glove box techniques, unless otherwise stated. The solvents acetonitrile (MeCN), dichloromethane (DCM), tetrahydrofuran (THF) and toluene were dried according to modified literature procedures. In brief, MeCN was distilled over P_2O_5 and CaH_2 in succession. DCM was dried by distillation over CaH_2 under argon, THF was distilled over $LiAlH_4$ under argon, and toluene was distilled over finely divided sodium under argon.

The reagents benzamidine hydrochloride, *p*-fluorobenzonitrile, sodium hydride (NaH), *p*-methylthiobenzonitrile, sodium ethanethiolate, 1-propanethiol, 2-propanethiol (*iso*-propylthiol), 2-methyl-2-propanethiol (*tert*-butylthiol), trimethylsilyl chloride (TMSCl) and sulfur monochloride (S_2Cl_2) were purchased commercially and used without further purification. Triphenylantimony (Ph_3Sb) was purchased commercially and recrystallized from MeCN prior to use. The diethyl etherate of lithium bis(trimethylsilyl)amide $Li[(N(TMS)_2)]\bullet OEt_2$ was prepared and purified according to a literature procedure.[1]

NMR solvents were purchased commercially and used without further purification. ^{1}H-NMR spectra were collected at room temperature on a Bruker Avance 300 MHz spectrometer and referenced internally to the residual solvent signal.[2]

Fourier-transform infrared (FTIR) spectra were recorded on a Bruker Alpha spectrometer using a single reflectance Platinum II diamond ATR module. For convenience, all spectra are plotted as the normalized % transmittance versus wavenumber ($T = 10^{-A}$, where A is the absorbance; $A = \log(1/R)$ with R the reflectance for ATR-FTIR measurements without ATR correction).

Elemental analyses CHN were performed in house on an Elementar UNICUBE elemental analyzer. All samples were prepared under an argon atmosphere, using high-purity tin (Sn) capsules that were

pre-weighted and loaded with ~2 mg of sample before being mechanically sealed. Sample masses were determined by differences on a digital microanalytical balance (≤ 2 g) immediately before introduction into the sample chamber.

Thermal-gravimetric analysis (TGA) was performed on a Perkin Elmer STA 600 simultaneous thermal (TG/DSC) analyzer using open Pt pans under nitrogen atmosphere (40 mL min^{-1} flow rate), with heating rates of 10 K min^{-1} over 295–873 K, typically using 3–8 mg of sample for all DTDA radicals. Temperature and weight calibration were performed with an indium standard and a standard weight of 50 mg, respectively. Recorded TGA data were processed using Pyris Manager software (v. 13).

Differential scanning calorimetry (DSC) analysis was performed on a power compensating type Perkin Elmer 8500 series instrument using hermetically sealed 50 µl aluminium pan. All samples were prepared in an argon-filled glovebox, using highly crystalline samples obtained by repeated zone-refinement of vacuum (10^{-3} bar) sublimated DTDA radical, unless otherwise stated. The weight of the sample was obtained by difference on a digital micro-analytical balance. Repetitive heating and cooling scans were carried out under nitrogen atmosphere (50 mL min^{-1} flow rate) after device temperature calibration using two standards (n-decane and indium metal). Energy calibration was performed using an indium standard.

2 Synthetic Procedures

2.1 Phenyl-(1,2,3,5)-dithiadiazolyl, 1

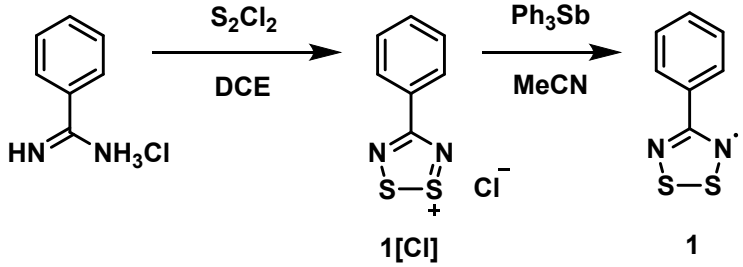

1[Cl] 1

Scheme S1. *Outline of the synthetic methodology leading to* ***1****.*

Synthesis of phenyl-(1,2,3,5)-dithiadiazolium chloride, 1[Cl]. To a well-stirred suspension of benzamidine hydrochloride (3.580 g, 22.87 mmol) in 45 mL DCE, cooled with an ice-water bath, was added a solution of sulfur monochloride (11.5 mL, 144 mmol) in 25 mL DCE. The resulting yellow-orange slurry was gently refluxed under argon overnight. The orange precipitate under a red solution was collected by hot filtration and washed with a mixture of 40 mL DCE and 10 mL carbon disulfide before drying *in vacuo*. Yield 93 % (4.597 g, 21.21 mmol). IR (ATR, cm^{-1}): 1595 (w), 1450 (m), 1391 (m), 1295 (m), 1236 (m), 1214 (m), 1170 (w), 1146 (m), 1067 (m), 1028 (m), 920 (m), 889 (s), 842 (m), 796 (m), 781 (m), 696 (s), 545 (m), 516 (w).

Synthesis of Phenyl-(1,2,3,5)-dithiadiazolyl, 1. A solution of triphenylantimony (3.191 g, 9.038 mmol) in 30 mL anhydrous, degassed (3 freeze-pump-thaw cycles) MeCN was poured onto phenyl-(1,2,3,5)-dithiadiazolium chloride (1.31 g, 6.05 mmol), and the dark purple mixture was refluxed under argon for 105 min. The solution was concentrated to about 10 mL before collecting the crystals by filtration and drying *in vacuo*. Crude yield 79 % (870 mg, 4.80 mmol). Purified by recrystallization from MeCN followed by three-zone gradient sublimation. IR (ATR, cm^{-1}): 1598 (w), 1538 (w), 1452 (m), 1371 (s), 1359 (s), 1321 (m), 1238 (m), 1225 (m), 1178 (m), 1136 (m), 1075 (m), 1000 (m), 982 (m), 922 (m), 899 (m), 836 (m), 802 (m), 775 (s), 765 (s), 684 (s), 653 (s), 506 (s). Anal. Calcd. (found): C, 46.39 (46.51); H, 2.78 (2.95); N, 15.46 (15.63).

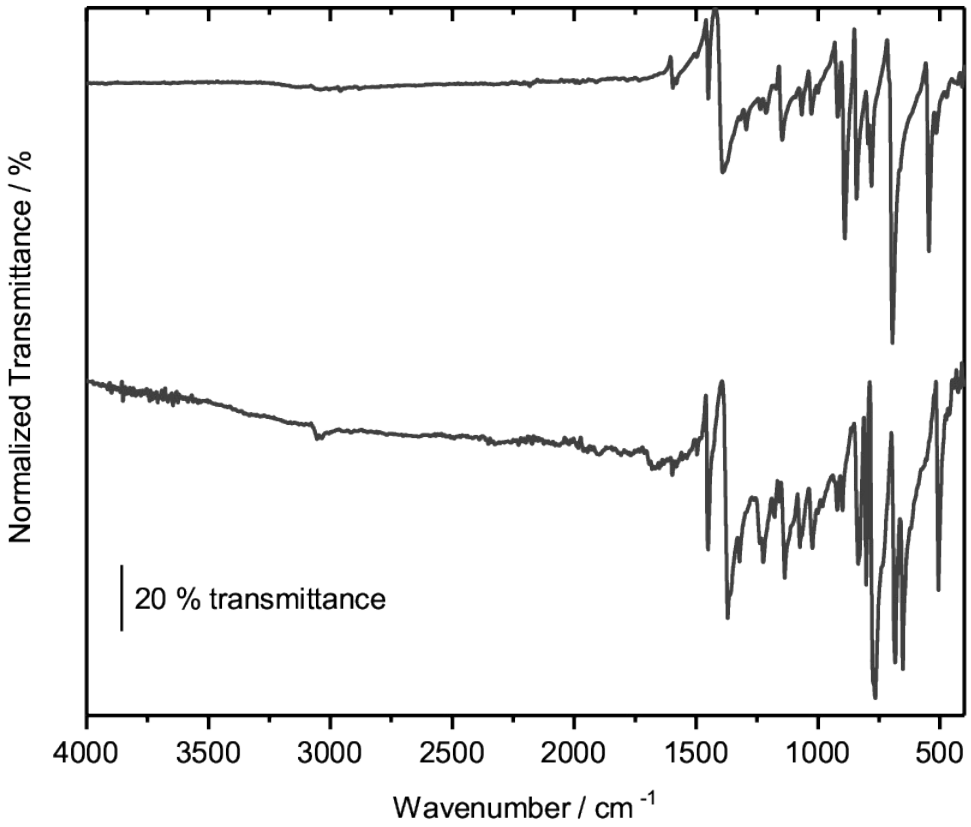

Figure S1. *Comparison of the FTIR spectra of* ***1[Cl]*** *(top) and* ***1*** *(bottom).*

2.2 *p*-(methylthio)-phenyl-(1,2,3,5)-dithiadiazolyl, 2

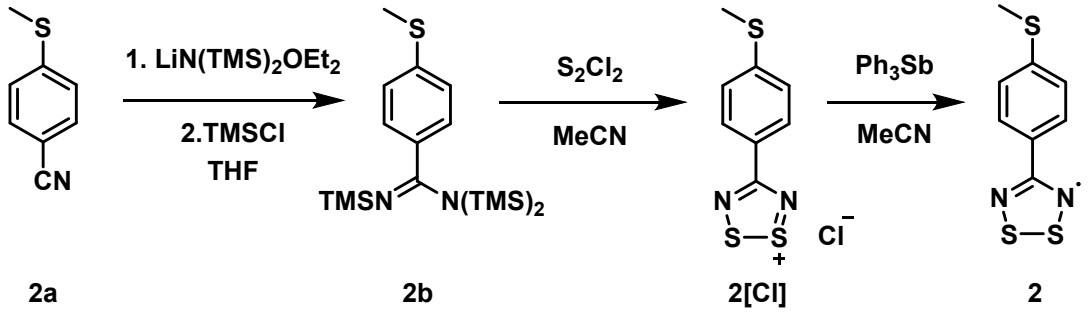

Scheme S2. *Outline of the synthetic methodology leading to* ***2****.*

Synthesis of N,N,N'-tris(trimethylsilyl)-*p*-(methylthio)-benzamidine, 2b. A solution of $LiN(TMS)_2 \bullet Et_2O$ (9.007 g, 37.304 mmol) in 80 mL of THF was added dropwise to a cold solution (ice-water bath) of *p*-methylthiobenzonitrile (**2a**, 5.496 g, 36.834 mmol) dissolved in 60 mL of THF. The mixture was stirred and allowed to warm to room temperature over 6 h and then the yellow solution was refluxed for 18 h. TMSCl (4.8 mL; 4.109 g, 37.820 mmol) was added to the solution and the mixture gently refluxed for 12 h to afford a dark yellow solution over a white precipitate of LiCl. The volatiles were flash distilled to afford a viscous yellow oil over a white solid. The oil was extracted twice with 2 x 40 mL of diethyl ether and canula filtered. The ether was evaporated under a strong flow of argon, and the resulting viscous yellow-orange oil was purified by fractional vacuum distillation, collecting the fraction distilling between 377 – 380K at 2 x 10^{-3} mbar. Collected 9.189 g. Yield 78 % based on consumed *p*-MeS-PhCN (24.005 mmol). ^{1}H-NMR (CD_2Cl_2, ppm): δ 7.276–7.179 (multiplet, 4H), 2.505 (singlet, 3H), 0.107 (singlet, 27 H). Decoupled ^{13}C-NMR (CD_2Cl_2, ppm): δ 168.45, 140.67, 129.32, 127.49, 126.07, 125.48, 15.71, 2.88.

Synthesis of *p*-(methylthio)-phenyl-(1,2,3,5)-dithiadiazolium chloride, 2[Cl]. To a cold solution (ice-water bath) of **2b** (3.529 g, 9.219 mmol) in 40 mL of MeCN was added dropwise sulfur monochloride (4.2 mL, 7.1 g, 53 mmol) in 20 mL of MeCN to afford an orange solid. The mixture was allowed to warm to room temperature and stirred at room temperature for 4 h. The precipitate was collected by filtration, washing with 2 x 30 mL of MeCN, 20 mL of hot DCE, 40 mL of DCM, and then dried in vacuo to afford crude **2[Cl]**. Yield 95 % (2.309 g, 8.786 mmol). IR (ATR, cm^{-1}): 2975 (w), 2899 (w), 1627 (w), 1585 (m), 1470 (w), 1403 (m), 1384 (s), 1360 (s), 1301 (m), 1228 (m), 1175 (m), 1138 (s), 1116 (m), 1087 (m), 1004 (m), 971 (m), 926 (m), 883 (m), 828 (s), 726 (s), 711 (m), 681 (s), 630 (m), 550 (s), 518 (w), 498 (m), 424 (m).

Synthesis of *p*-(methylthio)-phenyl-1,2,3,5-dithiadiazolyl, 2. A solution of triphenylantimony (3.116 g, 8.786 mmol) in 40 mL of MeCN was poured onto solid, crude **2[Cl]** (2.290 g, 8.714 mmol). The mixture was gently refluxed for 30 min under argon to afford a dark orange-brown solution over a greenish-black precipitate. The reaction mixture was cooled to room temperature and concentrated to ca. 20 mL, then cooled to 253 K to afford a heavy green-black precipitate which was collected by filtration, washed with 2 x 5 mL cold MeCN and dried *in vacuo*. Crude yield 95 % (1.903 g, 8.371 mmol). The material was purified by three-zone gradient sublimation at 303-323-353 K at 10^{-2} mbar. IR (ATR, cm^{-1}): 3034 (w), 2913 (w), 1911 (w), 1589 (m), 1493 (m), 1401 (m), 1371 (s), 1360 (s), 1323 (m), 1283 (m), 1237 (m), 1187 (m), 1136 (s), 1111 (s), 1088 (s), 1013 (m), 960 (m), 901 (m), 832 (m), 817 (s), 832 (s), 771 (s), 718 (s), 705 (m), 650 (s), 630 (m), 567 (m), 521 (w), 507 (s), 484 (s), 446 (w), 418 (m). Anal. Calcd. (found): C, 42.27 (42.71); H, 3.10 (3.257); N, 12.32 (12.37).

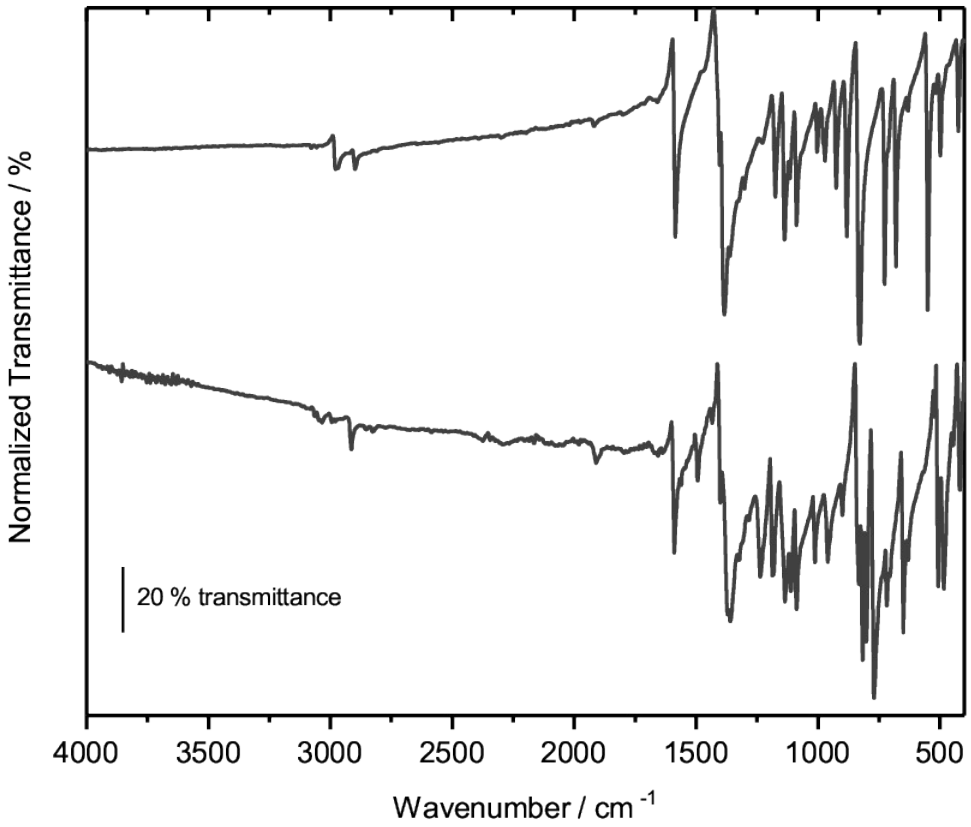

Figure S2. *Comparison of the FTIR spectra of* ***2[Cl]*** *(top) and* ***2*** *(bottom).*

2.3 *p*-(ethylthio)-phenyl-(1,2,3,5)-dithiadiazolyl, 3

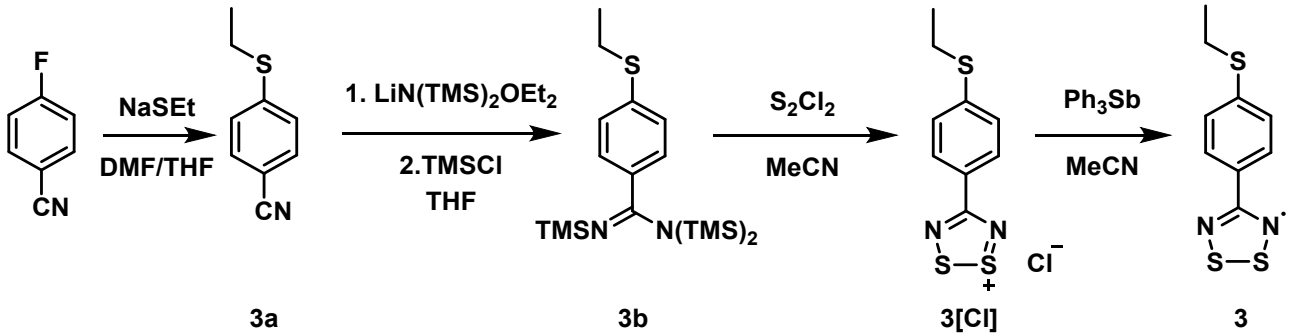

Scheme S3. *Outline of the synthetic methodology leading to* ***3****.*

Synthesis of *p*-(ethylthio)-benzonitrile, 3a. Reagent grade sodium ethanethiolate (6.403 g, 76.127 mmol) was dissolved in 60 mL of DMF and added dropwise to a solution of *p*-fluorobenzonitrile (8.308 g, 68.599 mmol) in 60 mL of THF and the mixture gently warmed to 353 K with stirring to afford a pale-yellow solution. After 6 h the solution was cooled, concentrated under reduced pressure and 80 mL of distilled water was added. The aqueous mixture was extracted twice with 40 mL DCM and the organic phase washed with 2 x 70 mL water, 150 mL of brine and then dried over $MgSO_4 \bullet H_2O$. The solids were removed by filtration and the organic phase was concentrated to afford a yellow liquid. Collected 11.047 g of crude (11.198 g expected based on *p*-fluorobenzonitrile). Purified by fractional vacuum distillation to afford a clear, colorless liquid, collecting the fraction distilling at 371 – 375K at 5.5 x 10^{-1} mbar. Yield 61 %. Collected 6.803 g, (41.675 mmol). ^{1}H-NMR (CD_2Cl_2, ppm): δ 7.527–7.492 (multiplet, 1.8 Hz, 4H), 3.002 (quartet, 7.5 Hz, 2H), 1.337 (triplet, 7.5 Hz, 3H). Decoupled ^{13}C-NMR (CD_2Cl_2, ppm): δ 145.31, 132.42, 126.82, 119.07, 108.13, 26.15, 13.84. IR (ATR, cm^{-1}): 2972 (w), 2929 (w), 2872 (w), 2223 (s), 1593 (s), 1593 (s), 1485 (s), 1450 (m), 1399 (m), 1379 (w), 1265 (m), 1179 (w), 1122 (w), 1087 (s), 1053 (w), 1014 (w), 969 (w), 818 (s), 793 (m), 779 (m), 764 (m), 708 (w), 669 (w), 640 (w), 589 (m), 577 (m), 541 (s), 445 (w), 406 (w).

Synthesis of *p*-(ethylthio)-benzamidine, 3b. To a cold solution (ice-water bath) of **3a** (3.287 g, 20.136 mmol) in 40 mL of THF was added dropwise a solution of $LiN(TMS)_2 \bullet Et_2O$ (5.034 g, 20.849 mmol) in 70 mL of THF. The mixture was stirred at room temperature for 24 h and then refluxed for 6 h under argon to afford a dark yellow solution which was cooled to room temperature before adding 2.6 mL of neat TMSCl (2.236 g, 20.582 mmol). The mixture was refluxed for 12 h and then the volatiles flash distilled to afford a dark orange viscous oil over a white solid. Diethyl ether (40 mL) was added to the mixture and the soluble fraction collected by canula filtration and the volatiles removed under reduced pressure. The crude, viscous brown oil was purified by fractional vacuum

distillation to afford a clear, yellow, viscous oil that distils at 394–397 K at 1.6 x 10^{-2} bar. Collected 3.291 g. Yield 41 % (8.293 mmol). ^{1}H-NMR (CD_2Cl_2, ppm): δ 7.256–7.231 (multiplet, 4H), 3.002 (quartet, 7.5 Hz, 2H), 1.310 (triplet, 7.5 Hz, 3H), 0.062 (singlet, 27H).

Synthesis of *p*-(ethylthio)-phenyl-(1,2,3,5)-dithiadiazolium chloride, 3[Cl]. To a cold solution (ice-water bath) of **3b** (3.175 g, 8.001 mmol) in 60 mL of MeCN was added dropwise sulfur monochloride (3.8 mL, 6.491 g, 48.006 mmol) in 20 mL of MeCN to afford a heavy bluish-beige solid. The mixture was allowed to warm to room temperature and gently refluxed for 15 minutes before collecting the grey-black precipitate by filtration, washing with 60 mL of MeCN, gently warming with 50 mL of DCE before allowing to cool to room temperature before filtering and finally washing with 3 x 40 mL of DCM, then dried in vacuo to afford a crude bluish-gray solid of crude **3[Cl]**. Collected 2.027 g (92 % Yield, 7.322 mmol). IR (ATR, cm^{-1}): 3076 (w), 2972 (w), 2923 (w), 2903 (w), 1934 (w), 1813 (w), 1673 (w), 1589 (m), 1536 (w), 1477 (w), 1442 (w), 1391 (s), 1368 (s), 1310 (m), 1252 (m), 1207 (w), 1183 (m), 1148 (m), 1118 (m), 1089 (m), 1052 (w), 1006 (m), 970 (w), 937 (w), 918 (w), 885 (m), 832 (s), 798 (m), 832 (s), 798 (m), 730 (s), 683 (m), 628 (w), 547 (m), 522 (w), 498 (m), 463 (w), 424 (w).

Synthesis of *p*-(ethylthio)-phenyl-(1,2,3,5)-dithiadiazolyl, 3. A solution of triphenylantimony (2.583 g, 7.316 mmol) in 40 mL of degassed MeCN was poured onto solid **3[Cl]** (2.004 g), 7.239 mmol). The mixture was refluxed for 30 minutes under argon to afford a dark orange solution over a small amount of yellowish-white solid. The mixture was hot filtered and concentrated to 20 mL before collecting the bronzy-black precipitate by filtration. The solid was washed with 20 mL of MeCN and dried in vacuo. Collected 1.308 g of crude **3** (75 % yield, 5.419 mmol). Two different crystal phases were obtained from MeCN; Lustrous green blocks and pale orange plates. Purified by three-zone temperature gradient (303-343-363 K) vacuum sublimation at 9 x 10^{-3} mbar to afford dark orange needles. IR (ATR, cm^{-1}): 3060 (w), 2964 (w), 2921 (w), 1903 (w), 1650 (w), 1589 (w), 1532 (m),

1493 (m), 1477 (m), 1438 (m), 1399 (m), 1367 (s), 1354 (s), 1259 (m), 1234 (m), 1181 (m), 1132 (s), 1108 (m), 1085 (s), 1055 (m), 1010 (s), 975 (m), 963 (m), 948 (m), 900 (m), 824 (s), 804 (s), 771 (s), 716 (s), 649 (s), 505 (s), 483 (m), 416 (m). Anal. Calcd. (Found): C, 44.79 (45.44); H, 3.76 (3.884); N, 11.61 (11.59).

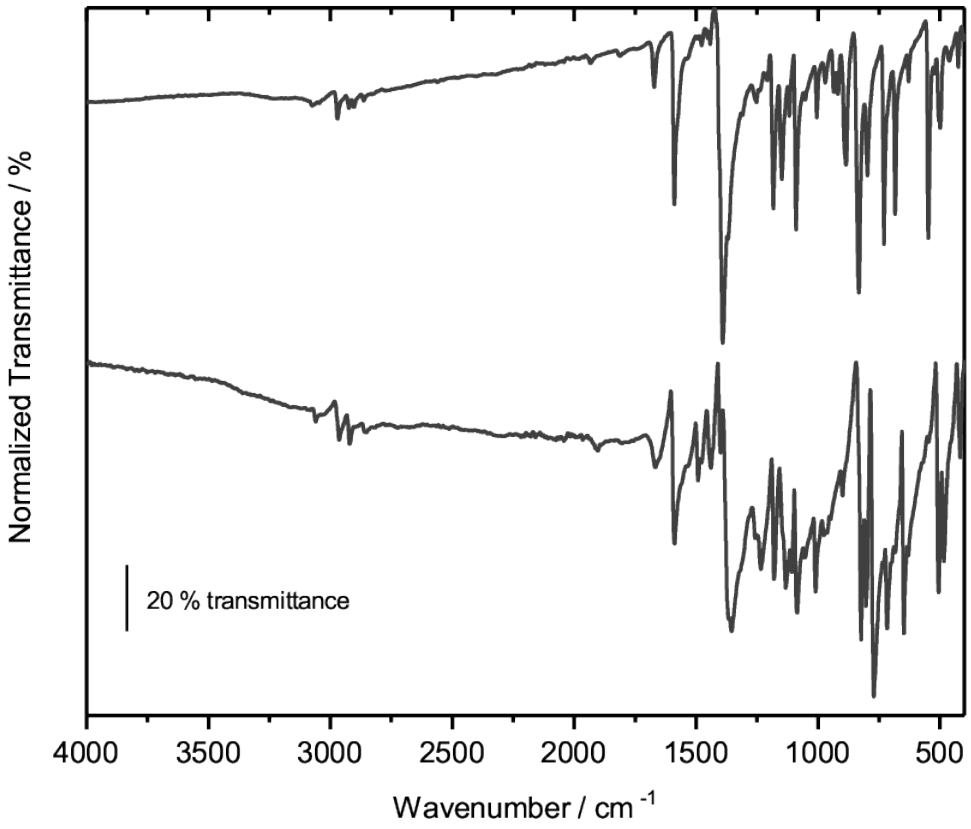

Figure S3. *Comparison of the FTIR spectra of* ***3[Cl]*** *(top) and* ***3α/3β*** *(bottom).*

2.4 *p*-(propylthio)-phenyl-(1,2,3,5)-dithiadiazolyl, 4

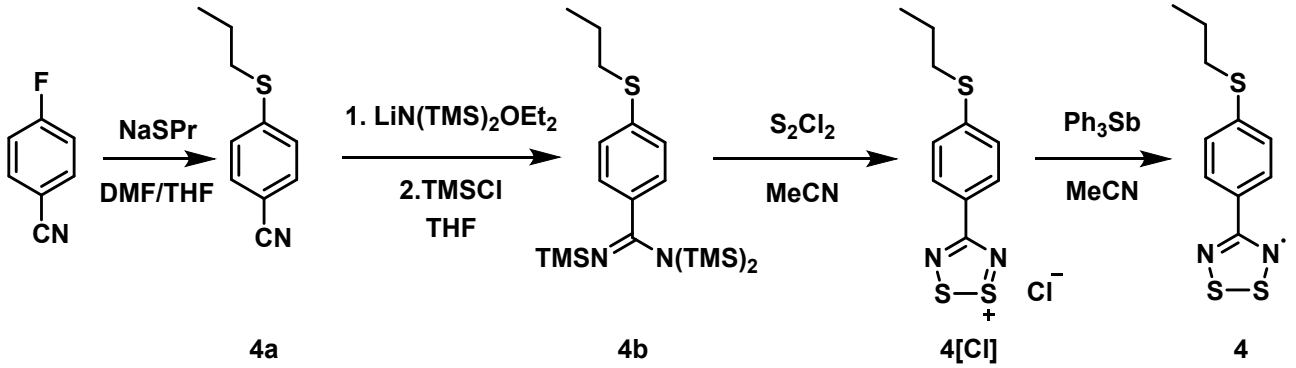

Scheme S4. *Outline of the synthetic methodology leading to **4**.*

Synthesis of *p*-(propylthio)-benzonitrile, 4a. Neat *n*-propylthiol (9.5 mL, 7.98 g, 104.78 mmol) was added dropwise to a suspension of NaH (2.572 g, 107.17 mmol) in 160 mL of THF and the mixture stirred at room temperature for 2 hours to afford a thick white suspension of sodium *n*-propylthiolate. Solid *p*-fluorobenzonitrile (12.594 g, 103.99 mmol) was added to the mixture with 40 mL of DMF added with stirring to afford a pale-yellow solution. After stirring for 16 h the solution was concentrated under reduced pressure and poured onto 200 mL of distilled water. The aqueous mixture was extracted twice with 130 mL of DCM and the organic phase washed with 3 x 100 mL of water, 100 mL of brine and then dried over $MgSO_4 \bullet H_2O$. The solids were removed by filtration and the organic phase was concentrated to afford a pale-yellow liquid. Purified by fractional vacuum distillation to afford a clear, colorless liquid, collecting the fraction distilling at 361–365 K at 3.0 x 10^{-1} mbar. Collected 14.258 g. Yield 77 % (80.431 mmol). ^{1}H NMR (CD_2Cl_2, ppm): δ 7.553–7.492 (multiplet, 1.8 Hz, 4H), 2.958 (triplet, 7.2 Hz, 2H), 1.713 (sextet, 7.2 Hz, 2H), 1.044 (triplet, 7.2 Hz, 3H). Decoupled ^{13}C-NMR (CD_2Cl_2, ppm): δ 145.61, 132.47, 126.98, 119.15, 108.20, 34.08, 22.39, 13.53. IR (ATR, cm^{-1}): 2964 (m), 2931 (w), 2872 (w), 2223 (s), 1591 (s), 1485 (m), 1458 (m), 1436 (w), 1340 (w), 1291 (w), 1238 (w), 1179 (w), 1122 (w), 1087 (s), 1014 (w), 895 (w), 816 (s), 779 (m), 747 (w), 708 (w), 579 (m), 541 (s), 445 (w).

Synthesis of N,N,N'-tris(trimethylsilyl)-*p*-(propylthio)-benzamidine, 4b. To a cold solution (ice-water bath) of **4a** (3.544 g, 19.992 mmol) in 40 mL of THF was added dropwise a solution of $LiN(TMS)_2 \bullet Et_2O$ (5.013 g, 20.726 mmol) in 70 mL of THF. The mixture was stirred at room temperature for 24 h and then refluxed for an additional 12 h and then the volatiles removed under reduced pressure to afford a crude, viscous brownish-yellow oil which was twice purified by fractional vacuum distillation, collecting the fraction distilling at 404–407 K at 2 x 10^{-2} mbar. Collected 3.550 g (43 % yield, 8.641 mmol). ^{1}H-NMR (CD_2Cl_2, ppm): δ 7.249–7.217 (multiplet, 4H), 2.927 (triplet, 7.2 Hz, 2H), 1.676 (sextet, 7.2 Hz, 2H), 1.024 (triplet, 7.2 Hz, 3H), 0.064 (singlet, 27 H).

Synthesis of *p*-(propylthio)-phenyl-(1,2,3,5)-dithiadiazolium chloride, 4[Cl]. To a cold (ice-water bath) of **4b** (3.550 g, 8.641 mmol) in 60 mL of MeCN was added dropwise sulfur monochloride (4.2 mL, 7.090 g, 52.508 mmol) in 20 mL of MeCN to afford a heavy bluish-beige solid. The mixture was allowed to warm to room temperature and gently refluxed for 1 h before collecting the grey-black precipitate by filtration, washing with 20 mL of MeCN, 50 mL of hot DCE and 3 x 30 mL of DCM, then dried in vacuo to afford a crude black solid of **4[Cl]**. Collected 2.215 g (88 % yield, 7.616 mmol). IR (ATR, cm^{-1}): 3074 (w), 2964 (w), 2921 (w), 2876 (w), 2856 (w), 1662 (w), 1585 (m), 1462 (w), 1432 (w), 1387 (s), 1371 (s), 1236 (m), 1208 (w), 1181 (m), 1152 (m), 1118 (m), 1091 (s), 1006 (m), 918 (m), 889 (m), 840 (s), 830 (m), 751 (m), 728 (s), 685 (m), 628 (w), 546 (m), 526 (w), 500 (m), 465 (w), 426 (w).

Synthesis of *p*-(propylthio)-phenyl-(1,2,3,5)-dithiadiazolyl, 4. A solution of triphenylantimony (1.416 g, 4.010 mmol) in 30 mL of degassed MeCN was poured onto solid **4[Cl]** (1.154 g, 3.968 mmol). The mixture was refluxed for 1 h under argon to afford a dark reddish-orange solution over a small amount of white solid. The mixture was hot filtered and concentrated to 20 mL before collecting the bronzy-black solid by filtration. The solid was washed with 10 mL of MeCN and dried in vacuo.

Collected 0.854 g (3.344 mmol) of crude **4**. Yield 84 %. Purified by repeat three-zone temperature gradient (303-323-343 K) vacuum sublimation at 1 x 10^{-2} mbar to afford dark orange plates. IR (ATR, cm^{-1}): 3033 (w), 2956 (m), 2927 (w), 2868 (w), 1907 (w), 1808 (w), 1656 (w), 1591 (m), 1493 (m), 1477 (w), 1460 (m), 1434 (w), 1403 (m), 1370 (m), 1358 (s), 1236 (m), 1187 (m), 1134 (s), 1058 (m), 900 (m), 820 (s), 800 (m), 769 (s), 730 (m), 718 (m), 647 (s), 549 (w), 504 (s), 481 (m), 455 (m), 426 (w), 412 (w). Anal. Calcd. (Found): C, 47.03 (46.86); H, 4.34 (4.41); N, 10.97 (10.86).

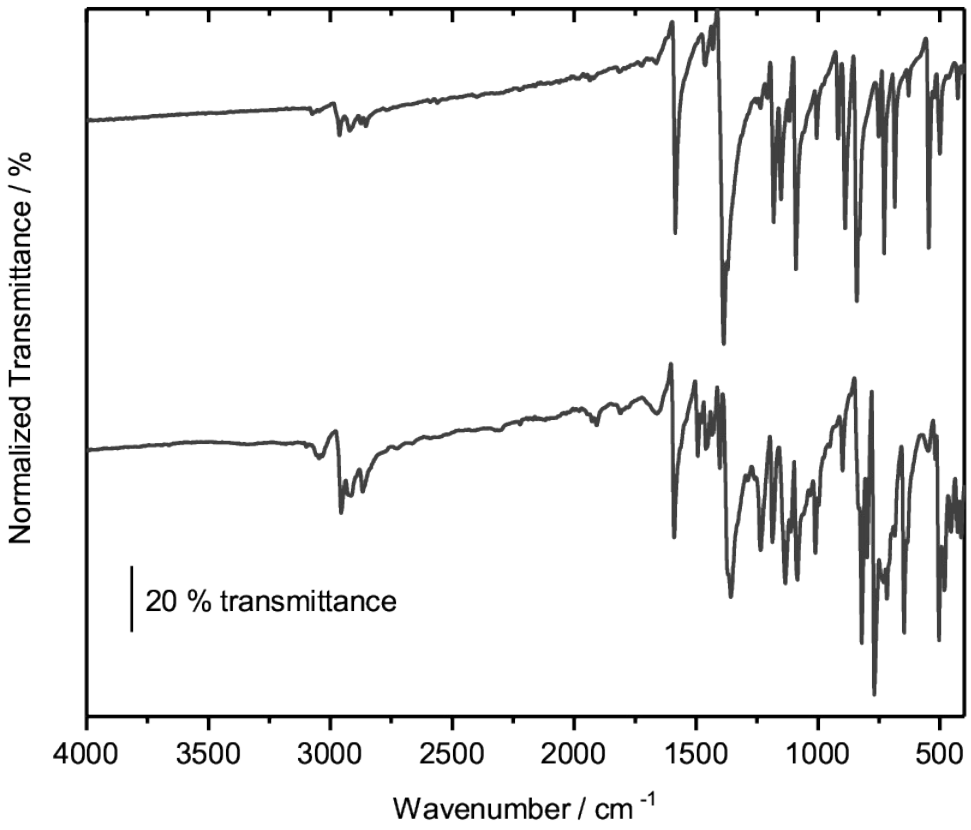

Figure S4. *Comparison of FTIR spectra of* ***4[Cl]*** *(top) and* ***4*** *(bottom).*

2.5 *p*-(isopropylthio)-phenyl-(1,2,3,5)-dithiadiazolyl, 5

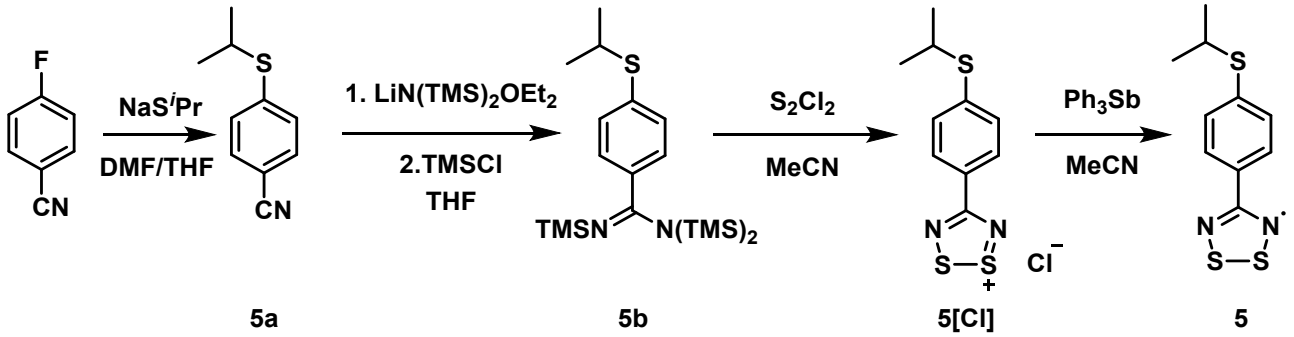

Scheme S5. *Outline of the synthetic methodology leading to* ***5****.*

Preparation of *p*-(isopropylthio)-benzonitrile, 5a. Neat isopropylthiol (9.30 mL, 7.63 g, 100.13 mmol) was added dropwise to a suspension of NaH (2.496 g, 0.104 mmol) in 160 mL of THF and the mixture stirred at room temperature for 4 h to afford a thick white suspension of sodium isopropylthiolate. To this suspension was slowly canula transferred a solution of *p*-fluorobenzonitrile (12.174 g, 100.52 mmol) in 80 mL of a 1:1 mixture of THF and DMF and the mixture warmed to 353 K with stirring to afford a pale-yellow solution. After 16 h the solution was cooled, concentrated in vacuum and 100 mL of distilled water added. The aqueous mixture was extracted twice with 80 mL of DCM and the organic phase was washed with 3 x 100 mL of water, 100 mL of brine, and then dried over $MgSO_4 \bullet H_2O$. The solids were removed by filtration and the organic phase was concentrated to afford a pale-yellow liquid. Purified by fractional vacuum distillation to afford a clear, colorless liquid, collecting the fraction distilling at 355–359 K at 4.6 x 10^{-2} mbar. Collected 12.413 g. Yield 70 % (70.023 mmol). ^{1}H-NMR (CD_2Cl_2, ppm): δ 7.535–7.501 (multiplet, 1.8 Hz, 2H), 7.340–7.312 (multiplet, 1.8 Hz, 2H), 3.538 (septet, 6.6 Hz, 1H), 1.329 (doublet, 6.6 Hz, 6H). Decoupled ^{13}C-NMR (CD_2Cl_2, ppm): δ 144.54, 132.43, 128.69, 118.97, 108.73, 36.70, 22.87. IR

(ATR, cm^{-1}): 2966 (m), 2927 (w), 2868 (w), 2225 (m), 1591 (s), 1485 (m), 1454 (m), 1403 (m), 1385 (m), 1369 (m), 1307 (w), 1244 (m), 1179 (w), 1154 (m), 1122 (w), 1087 (s), 1016 (m),953 (w), 034 (w), 879 (w), 818 (s), 779 (w), 710 (w), 655 (w), 636 (w), 592 (m), 543 (s), 447 (w).

Synthesis of N,N,N'-tris(trimethylsilyl)-*p*-(isopropylthio)-benzamidine, 5b. To a cold solution (ice-water bath) of **5a** (3.621 g, 20.426 mmol) in 40 mL of THF was added dropwise a solution of $LiN(TMS)_2 \bullet Et_2O$ (5.075 g, 21.019 mmol) in 70 mL of THF. The mixture was stirred at room temperature for 24 h and then refluxed for 6 h under argon to afford a dark yellow solution which was cooled to room temperature before adding 2.7 mL of neat TMSCl (2.322 g, 21.373 mmol). The mixture was refluxed for 12 h and then the volatiles flash distilled to afford an amber oil. The oil was purified by fractional vacuum distillation, collecting the yellow fraction distilling at 354–356 K at 8 x 10^{-3} mbar. Collected 4.615 g (55 % yield, 11.23 mmol). ^{1}H-NMR (CD_2Cl_2, ppm): δ 7.329–7.208 (dd (AA'XX'), 8.1 Hz, 4H), 3.428 (septet, 7.3 Hz, 1H), 1.288 (doublet, 7.3 Hz, 6H), 0.067 (singlet, 27H).

Synthesis of *p*-(isopropylthio)-phenyl-(1,2,3,5)-dithiadiazolium chloride, 5[Cl]. To a cold solution (ice-water bath) of **5b** (2.761 g, 6.720 mmol) in 40 mL of MeCN was added dropwise sulfur monochloride (3.4 mL, 5.7 g, 43 mmol) in 20 mL of MeCN to afford a heavy beige precipitate. The mixture was allowed to warm to room temperature and gently refluxed for 1 h before collecting the pale-orange precipitate by filtration, washing with 20 mL of MeCN to afford a beige solid. Refluxing the solid with 40 mL of DCE afforded a dark orange-brown solution which was hot filtered, concentrated to 25 mL and cooled to room temperature to afford a pale orange plate-like crystalline solid, which was collected by filtration and dried in vacuo. Yield 80%. Collected 1.567 g (5.388 mmol). IR (ATR, cm^{-1}): 2959 (w), 2922 (w), 2864 (w), 1646 (w), 1589 (m), 1495 (w), 1448 (w), 1391 (s), 1367 (s), 1281 (m), 1238 (m), 1185 (m), 1152 (m), 1087 (m), 1050 (m), 1012 (m), 924 (m), 891 (m), 826 (s), 728 (m), 683 (m), 653 (w), 628 (w), 545 (m), 496 (m), 465 (w), 426 (w).

Synthesis of *p*-(isopropylthio)-phenyl-(1,2,3,5)-dithiadiazolyl, 5. A solution of Ph_3Sb (1.063 g, 3.011 mmol) in 25 mL of MeCN was poured onto **5[Cl]** (0.883 g, 3.036 mmol) and the resulting mixture gently refluxed for 45 minutes before hot filtering and concentrating the solution to around 10 mL to afford a lustrous, black microcrystalline solid. The solid was collected by filtration and the residual solvent removed *in vacuo.* Collected 0.592 g (yield 77 %, 2.318 mmol). Sublimation from 313-323-353 K at 1.0 x 10^{-2} mbar afforded fine needle-like feathers. Collected 0.303 g of solid, plus recovered an additional 0.109 g of sticky crude material. IR (ATR, cm^{-1}): 3051 (w), 2956 (w), 2921 (w), 2860 (w), 1675 (w), 1589 (m), 1493 (w), 1446 (w), 1401 (m), 1358 (s), 1236 (m), 1183 (m), 1183 (m), 1134 (m), 1089 (m), 1048 (m), 1014 (m), 902 (w), 832 (m), 802 (m), 769 (s), 720 (m), 651 (m), 504 (m), 414 (w). Anal. Calcd. (Found): C, 47.03 (47.57); H, 4.34 (4.746); N, 11.61 (11.43).

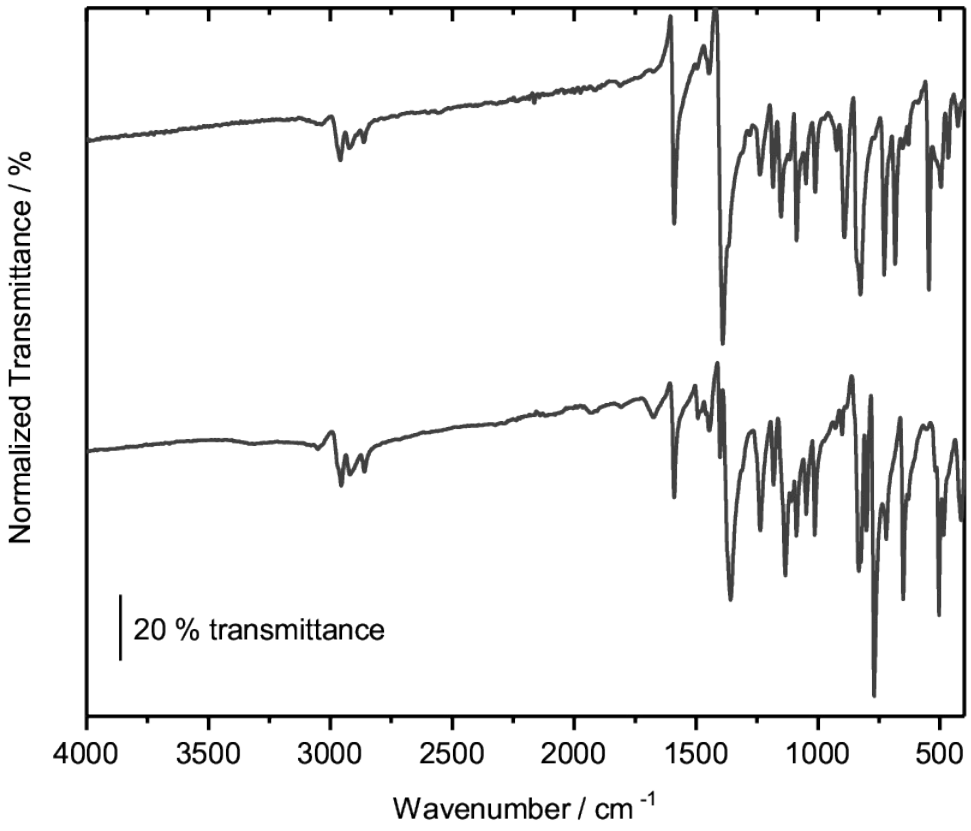

Figure S5. *Comparison of the FTIR spectra of* ***5[Cl]*** *(top) and* ***5*** *(bottom)*

2.6 *p*-(*tert*-butylthio)-phenyl-(1,2,3,5)-dithiadiazolyl, 6

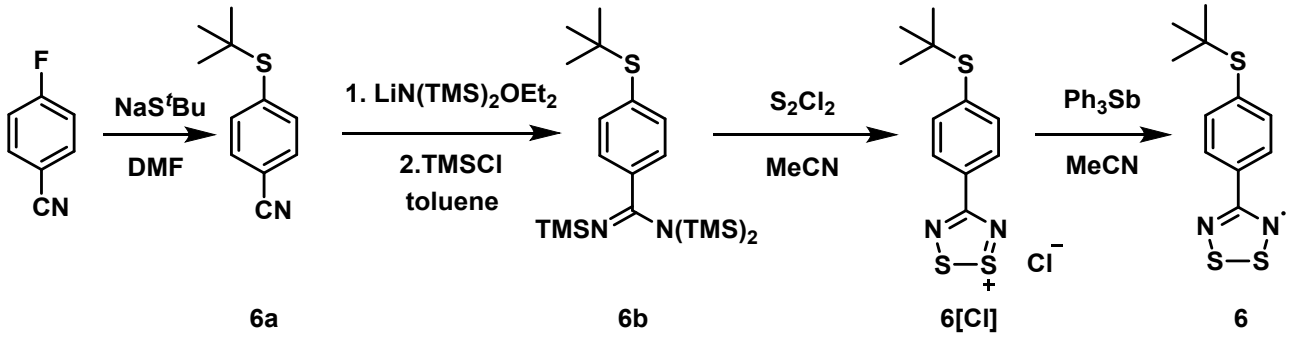

Scheme S6. *Outline of the synthetic methodology leading to* ***6****.*

Preparation of *p*-(*tert*-butylthio)-benzonitrile, 6a. To a mixture of *tert*-butylthiol (8.0 mL, 71 mmol) and sodium hydride (1.70 g, 70.9 mmol) was added dimethylformamide (DMF, 40 mL) at 273–278 K, and the resulting mixture was allowed to warm to room temperature over 8 h. *p*-fluorobenzonitrile (5.67 g, 46.8 mmol) was added, and the mixture was stirred at room temperature for 24 h. The mixture was poured into deionized water (200 mL) and extracted with $CHCl_3$ (2x 200 mL). The organic phase was separated, washed with water (2x 200 mL) and dried over $MgSO_4 \bullet H_2O$. The $CHCl_3$ was removed at reduced pressure to afford a clear, colorless oil which was purified by fractional distillation at 333 K, 10^{-2} mbar. Yield 78 % (6.99 g). ^{1}H NMR (300 MHz, $CDCl_3$): 7.61 (doublet, 1.80 Hz, 4H), 1.32 (singlet, 9H).

Preparation of N,N,N'-tris(trimethylsilyl)-*p*-(*tert*-butylthio)-benzamidine, 6b. A solution of $LiN(TMS)_2 \bullet Et_2O$ (5.68 g, 23.5 mmol) in toluene (75 mL) was added dropwise to a solution of **6a** (4.50 g, 23.5 mmol) in toluene (50 mL), at 273–278 K. The mixture was stirred and allowed to warm to room temperature over 24h. The resulting mixture was refluxed for 2 h, cooled down to room

temperature, and TMSCl (3.0 mL, 24 mmol) was added. The mixture was refluxed for 24 h. The resulting white precipitate was removed by filtration and the solvent was removed by flash distillation. The crude material was recrystallized at 253 K from MeCN (50 mL) to afford clear, colorless needles. Yield 32 % (4.04 g, 9.51 mmol). ^{1}H NMR (300 MHz, $CDCl_3$): 7.46 (doublet, 8.4 Hz, 2H), 7.23 (doublet, 8.4 Hz, 2H), 1.28 (singlet, 9H), 0.06 (singlet, 27H).

Preparation of *p*-(*tert*-butylthio)-phenyl-1,2,3,5-dithiadiazolium chloride, 6[Cl]. Sulfur monochloride (2.3 mL, 29 mmol) in MeCN (30 mL) was added dropwise to a solution of **6b** (1.90 g, 4.46 mmol) in MeCN (50 mL) at 273–278 K. The mixture was stirred for 4 h, and the resulting precipitate was collected by filtration and washed with MeCN (50 mL) and DCM (2 x 50 mL). Yield 71 % (0.970 g, 3.18 mmol). IR (ATR, cm^{-1}): 2962 (w), 1673 (w), 1587 (m), 1469 (w), 1391 (s), 1364 (m), 1309 (w), 1281 (w), 1228 (w), 1183 (m), 1152 (m), 1112 (w), 1073 (m), 1012 (m), 922 (w), 891 (m), 842 (m), 830 (m), 728 (m), 683 (m), 665 (m), 545 (m), 514 (w), 500 (w), 445 (m), 420 (w).

Preparation of *p*-(*tert*-butylthio)-phenyl-1,2,3,5-dithiazolyl, 6. A solution of Ph_3Sb (1.53 g, 4.33 mmol) in MeCN (40 mL) was degassed by three freeze-pump-thaw cycles and poured over solid **6[Cl]** (2.20 g, 7.22 mmol). The resulting mixture was stirred at room temperature for 1 h, and the resulting precipitate was collected by filtration and washed with MeCN (15 mL). The resulting solution was concentrated to 25 mL and kept at 253 K over 4 h, and the resulting crystals were collected by filtration. The crystals were further purified by vacuum sublimations over three-zone temperature gradient (303-333-353 K). Yield: 7.2 % (0.14 g 0.52 mmol). IR (ATR, cm^{-1}): 2957 (w), 2937 (w), 2921 (w), 2892 (w), 2858 (w), 1671 (w), 1589 (w), 1469 (w), 1454 (w), 1401 (w), 1360 (m), 1242 (w), 1176 (m), 1134 (m), 1101 (m), 1016 (m), 934 (w), 902 (w), 842 (m), 826 (m), 803 (m), 771 (s), 732 (m), 685 (w), 653 (m), 632 (w), 583 (w), 530 (w), 506 (m), 485 (w), 455 (w), 410 (w). Anal. Calcd. (found): C, 49.04 (49.23), H, 4.86 (5.018), N, 10.40 (10.38).

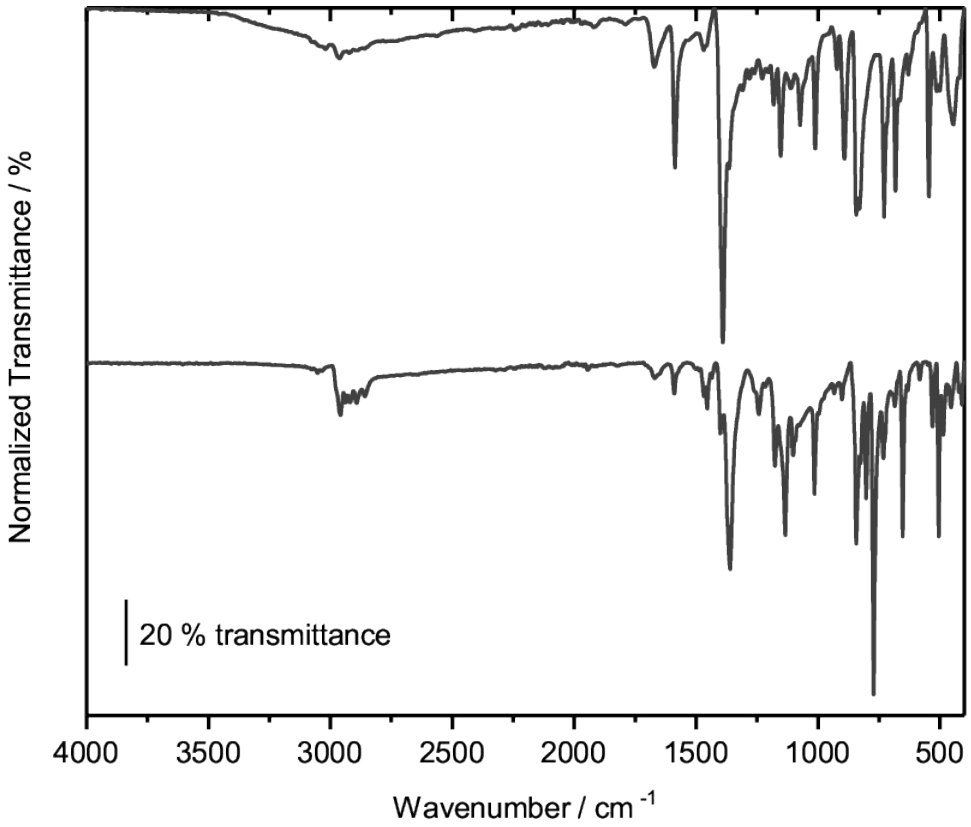

Figure S6. *Comparison of the FTIR spectra of* ***6[Cl]*** *(top) and* ***6*** *(bottom).*

Table S1. Summary of vacuum sublimation zone refinement temperatures and morphology of **1** – **6**.

	T_1 (K)	T_2 (K)	T_3 (K)	Appearance[#]/Morphology
1	303	308	321	violet needles
2	303	323[†]	353	green blocks
3α	303	343[†]	363	dark orange blocks
3β	285*[†]	359	-	orange plates
3γ	303[†]	343	363	orange plates
4	303	323[†]	343	dark orange plates
5	313	323[†]	353	fine needle-like clusters
6	303	333	353	purple needles

[#] Appearance under transmitted light. *Sublimed onto a water-cooled cold-finger; [†]Zone of deposition during sublimation.

3 Crystallography

3.1 Single-Crystal X-Ray Diffraction (SC-XRD) Measurements

Variable temperature single-crystal X-ray diffraction studies were collected either on an Agilent SuperNova equipped with multilayer optics monochromated dual source (Cu and Mo), Atlas detector, using Cu K_α (1.54184 Å) or Mo K_α (0.71073 Å) radiation, or with a Rigaku XtaLAB Synergy-R with a HyPix-Arc 100° detector and Cu K_α (1.54184 Å) rotating anode source. Crystals were mounted on MiTeGen micro-mounts using Fomblin oil. Data acquisitions, reductions and analytical face- and index based absorption corrections were made using CrysAlis^{PRO}.[3] The structures were solved using ShelXT[4] and refined on F^2 by full matrix least-squares techniques with ShelXL[5,6] included in the OLEX2[7] program package.

Table S2. Single crystal parameters for **1** and **2**.

	1	**2**

Empirical formula	$C_7H_5N_2S_2$	$C_8H_7N_2S_3$
Formula weight	181.25	227.34
Temperature/K	120	293(2)
Crystal system	orthorhombic	monoclinic
Space group	$P2_12_12_1$	$P2_1$
a/Å	5.74890(10)	5.74270(10)
b/Å	16.0651(3)	17.4995(2)
c/Å	32.9763(5)	9.65670(10)
α/°	90	90
β/°	90	101.7890(10)
γ/°	90	90
Volume/Å^3	3045.58(9)	949.97(2)
Z	16	4
ρ_{calc}g/cm^3	1.581	1.59
μ/mm^{-1}	5.736	6.729
F(000)	1488	468
Crystal size/mm^3	0.231 × 0.023 × 0.016	0.06 × 0.05 × 0.03
Radiation	CuKα (λ = 1.54184)	CuKα (λ = 1.54184)
2Θ range for data collection/°	5.36 to 157.568	9.356 to 149.004
Index ranges	$-7 \le h \le 7$, $-20 \le k \le 19$, $-33 \le l \le 41$	$-6 \le h \le 7$, $-21 \le k \le 21$, $-12 \le l \le 12$
Reflections collected	32210	99043
Independent reflections	6270 [R_{int} = 0.0362, R_{sigma} = 0.0271]	3882 [R_{int} = 0.0221, R_{sigma} = 0.0064]
Data/restraints/parameters	6270/0/397	3882/1/238
Goodness-of-fit on F^2	1.023	1.056
Final R indexes [I>=2σ (I)]	R_1 = 0.0264, wR_2 = 0.0676	R_1 = 0.0164, wR_2 = 0.0473
Final R indexes [all data]	R_1 = 0.0306, wR_2 = 0.0694	R_1 = 0.0166, wR_2 = 0.0474
Largest diff. peak/hole / e Å^{-3}	0.20/-0.22	0.13/-0.12
Flack parameter	-0.008(7)	0.067(12)

Table S3. Single crystal parameters for **3**α, **3**β and **3**γ.

	3α	**3β**	**3γ**
Empirical formula	$C_9H_9N_2S_3$	$C_9H_9N_2S_3$	$C_9H_9N_2S_3$
Formula weight	241.36	241.36	241.36
Temperature/K	300.00(10)	300.00(10)	300.15
Crystal system	monoclinic	monoclinic	monoclinic
Space group	$P2_1/c$	Pn	$P2_1/n$
a/Å	12.6651(3)	5.6566(2)	5.7190(3)
b/Å	15.7806(3)	20.2060(5)	41.353(3)
c/Å	11.4706(3)	9.3436(3)	9.3267(4)
α/°	90	90	90
β/°	111.534(3)	103.844(3)	103.459(5)
γ/°	90	90	90
Volume/Å^3	2132.53(9)	1036.92(6)	2145.1(2)
Z	8	4	8
ρ_{calc}g/cm^3	1.504	1.546	1.495
μ/mm^{-1}	6.029	6.199	5.993
F(000)	1000	500	1000
Crystal size/mm^3	0.091 × 0.089 × 0.042	0.162 × 0.113 × 0.009	0.099 × 0.082 × 0.006
Radiation	CuKα (λ = 1.54184)	CuKα (λ = 1.54184)	CuKα (λ = 1.54184)
2Θ range for data collection/°	7.504 to 148.914	4.374 to 148.976	8.554 to 148.916
Index ranges	-15 ≤ h ≤ 15, -19 ≤ k ≤ 18, -14 ≤ l ≤ 14	-6 ≤ h ≤ 7, -25 ≤ k ≤ 24, -11 ≤ l ≤ 11	-6 ≤ h ≤ 6, -48 ≤ k ≤ 48, -11 ≤ l ≤ 9
Reflections collected	40964	20012	31357
Independent reflections	4360 [R_{int} = 0.0358, R_{sigma} = 0.0187]	3911 [R_{int} = 0.0488, R_{sigma} = 0.0291]	4238 [R_{int} = 0.0857, R_{sigma} = 0.0323]
Data/restraints/parameters	4360/0/255	3911/2/256	3877/0/255
Goodness-of-fit on F^2	1.100	1.013	1.094
Final R indexes [I>=2σ (I)]	R_1 = 0.0311, wR_2 = 0.0881	R_1 = 0.0416, wR_2 = 0.1085	R_1 = 0.0760, wR_2 = 0.2024
Final R indexes [all data]	R_1 = 0.0341, wR_2 = 0.0966	R_1 = 0.0431, wR_2 = 0.1095	R_1 = 0.1043, wR_2 = 0.2309
Largest diff. peak/hole / e Å^{-3}	0.46/-0.42	0.60/-0.37	0.48/-0.53
Flack parameter		0.26(3)	

Table S4. Single crystal parameters for **4**, **5**, and **6**.

	4	**5**	**6**

Empirical formula	$C_{10}H_{11}N_2S_3$	$C_{10}H_{11}N_2S_3$	$C_{11}H_{13}N_2S_3$
Formula weight	255.39	255.39	269.41
Temperature/K	300.00(10)	273.15	300.00(10)
Crystal system	monoclinic	monoclinic	monoclinic
Space group	$P2_1/n$	$P2_1/c$	$P2_1/n$
a/Å	5.75410(10)	5.8238(2)	5.98820(10)
b/Å	45.2695(5)	43.3605(6)	44.9141(9)
c/Å	9.2598(2)	12.1776(4)	9.6438(2)
α/°	90	90	90
β/°	103.684(2)	128.977(5)	97.849(2)
γ/°	90	90	90
Volume/Å^3	2343.58(7)	2390.59(18)	2569.44(9)
Z	8	8	8
ρ_{calc}g/cm^3	1.448	1.419	1.393
μ/mm^{-1}	5.517	5.409	5.061
F(000)	1064	1064	1128
Crystal size/mm^3	0.177 × 0.116 × 0.02	0.211 × 0.16 × 0.035	0.249 × 0.074 × 0.016
Radiation	CuKα (λ = 1.54184)	CuKα (λ = 1.54184)	CuKα (λ = 1.54184)
2Θ range for data collection/°	7.812 to 149.006	4.076 to 148.998	7.874 to 148.962
Index ranges	$-7 \le h \le 7$, $-56 \le k \le 56$, $-10 \le l \le 11$	$-7 \le h \le 7$, $-54 \le k \le 54$, $-15 \le l \le 15$	$-7 \le h \le 7$, $-56 \le k \le 55$, $-11 \le l \le 12$
Reflections collected	319896	48950	74309
Independent reflections	4780 [R_{int} = 0.0754, R_{sigma} = 0.0101]	4883 [R_{int} = 0.0773, R_{sigma} = 0.0329]	5246 [R_{int} = 0.0483, R_{sigma} = 0.0188]
Data/restraints/parameters	4780/102/301	4884/3/289	5246/0/295
Goodness-of-fit on F^2	1.096	1.061	1.085
Final R indexes [I>=2σ (I)]	R_1 = 0.0486, wR_2 = 0.1410	R_1 = 0.0468, wR_2 = 0.1381	R_1 = 0.0404, wR_2 = 0.1010
Final R indexes [all data]	R_1 = 0.0510, wR_2 = 0.1426	R_1 = 0.0526, wR_2 = 0.1434	R_1 = 0.0456, wR_2 = 0.1039
Largest diff. peak/hole / e Å^{-3}	0.30/-0.34	0.36/-0.26	0.29/-0.26

3.2 Powder X-Ray Diffraction (PXRD) Measurements

Powder X-ray diffraction (PXRD) analyses were made using PANalytical X´Pert PRO diffractometer. Diffraction data were acquired using Cu K_α radiation (λ = 1.5418; tube settings 45 kV, 40 mA) and position-sensitive X´Celerator detector. Diffraction intensities were collected from a spinning sample using 2θ range of 2−60°, with step size of 0.017° and counting times varying per sample from 60 to 180 s to obtain sufficient diffraction intensities. A freshly crystallized and lightly hand-ground powder sample was prepared on an air- and moisture protecting domed sample holder, using petrolatum jelly as an adhesive. The diffractometer was aligned using a Si powder standard material (SRM 640, National Institute of Standards & Technology). Data processing and Pawley whole-pattern fits were made with the program X´pert HighScore Plus (v. 4.9). The unit cell parameters of the powder samples were refined by Pawley analysis using the corresponding single crystal structure parameters obtained in this study, as the basis of the least-squares refinements. Variables for the fits were as follows: zero-offset, polynomial background, sample displacement, unit cell parameters and peak profile parameters (peak width, shape, and asymmetry).

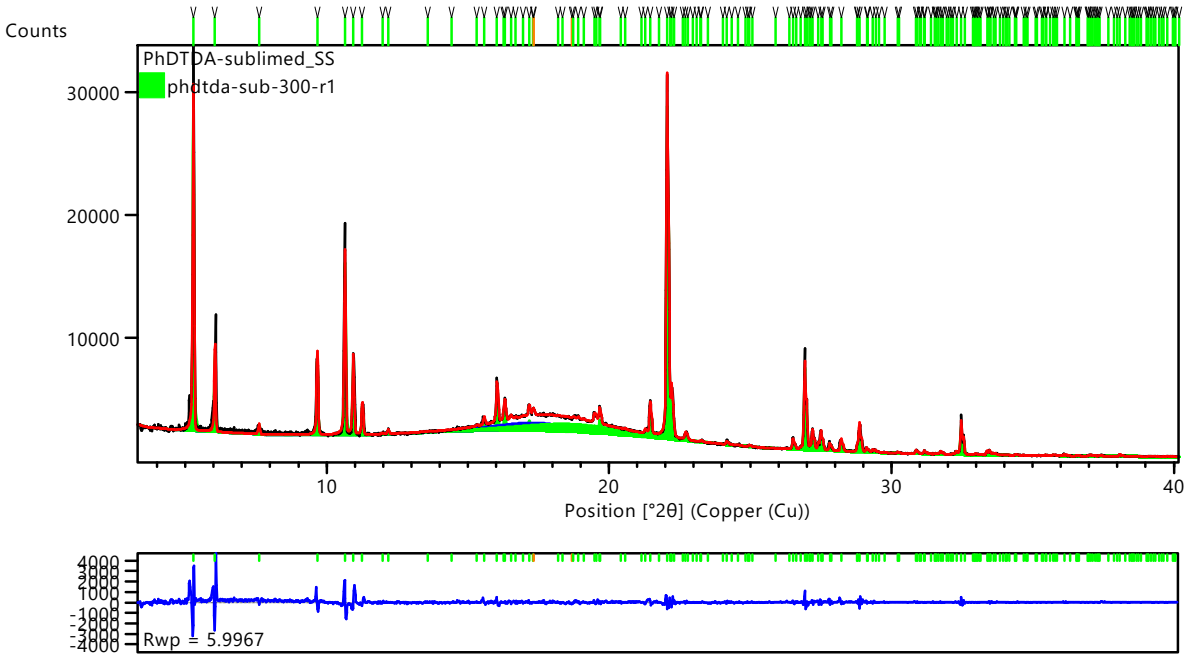

Figure S7. *Pawley refinement of **1**. Experimental pattern is shown in black, refined profile in red, while green-colored markers on top correspond to characteristic Bragg peak positions of the assigned phase. Difference plot of the experimental vs. refined profiles is shown below in blue. See Table S5.*

Table S5. Crystallographic data for **1**.

Parameters	PXRD	SC-XRD
Temperature (K)	293	300
Crystal system	orthorhombic	orthorhombic
Space group	$P2_12_12_1$	$P2_12_12_1$
a /Å	5.743(7)	5.74890(10)
b /Å	16.05(1)	16.0651(3)
c /Å	32.989(3)	32.9763(5)
α /°	90	90
β /°	90	90
γ /°	90	90
V/Å^3	3041.66	3045.58(9)
$R_{prof.}$	0.0458	
$R_{w\text{-}prof}$	0.0560	
GOF	2.288	

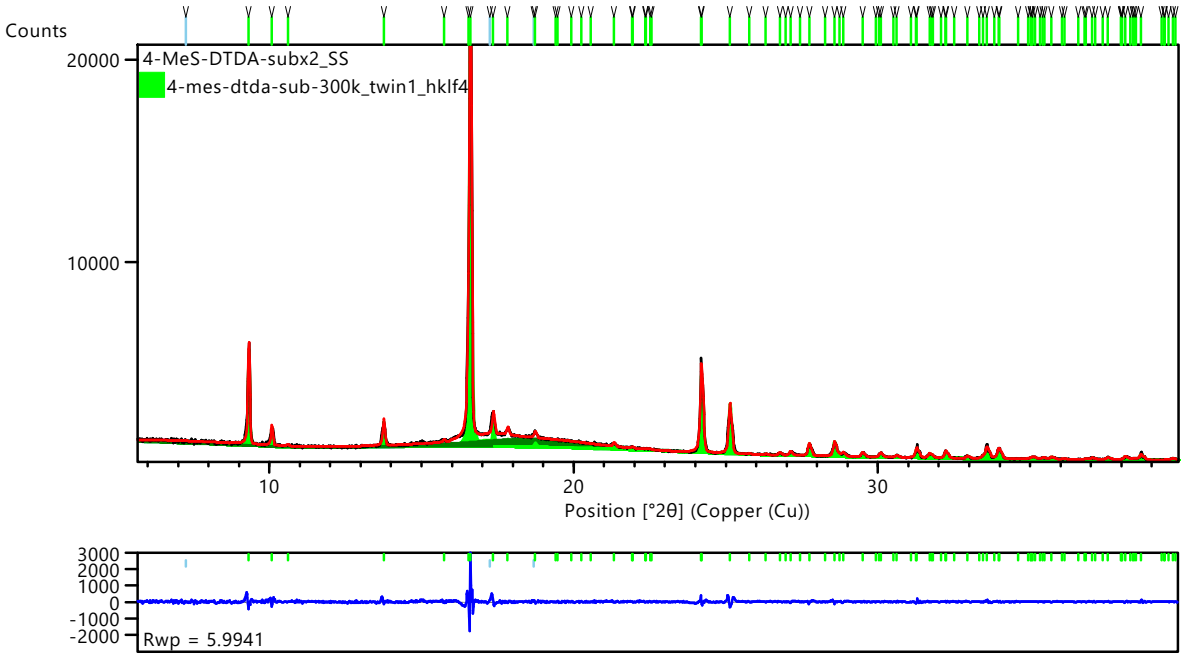

Figure S8. *Pawley refinement of **2**. Experimental pattern is shown in black, refined profile in red, while green-colored markers on top correspond to characteristic Bragg peak positions of the assigned phase. Difference plot of the experimental vs. refined profiles is shown below in blue. See Table S6.*

Table S6. Crystallographic data for **2**.

Parameters	PXRD	SC-XRD
Temperature (K)	293	300
Crystal system	monoclinic	monoclinic
Space group	$P2_1$	$P2_1$
a /Å	5.738(1)	5.74270(10)
b /Å	17.500(4)	17.4995(2))
c /Å	9.658(2)	9.65670(10)
α /°	90	90
β /°	101.741(1)	101.7890(10)
γ /°	90	90
V/Å^3	949.56	949.97(2)
$R_{prof.}$	0.0454	
$R_{w\text{-}prof}$	0.0560	
GOF	1.480	

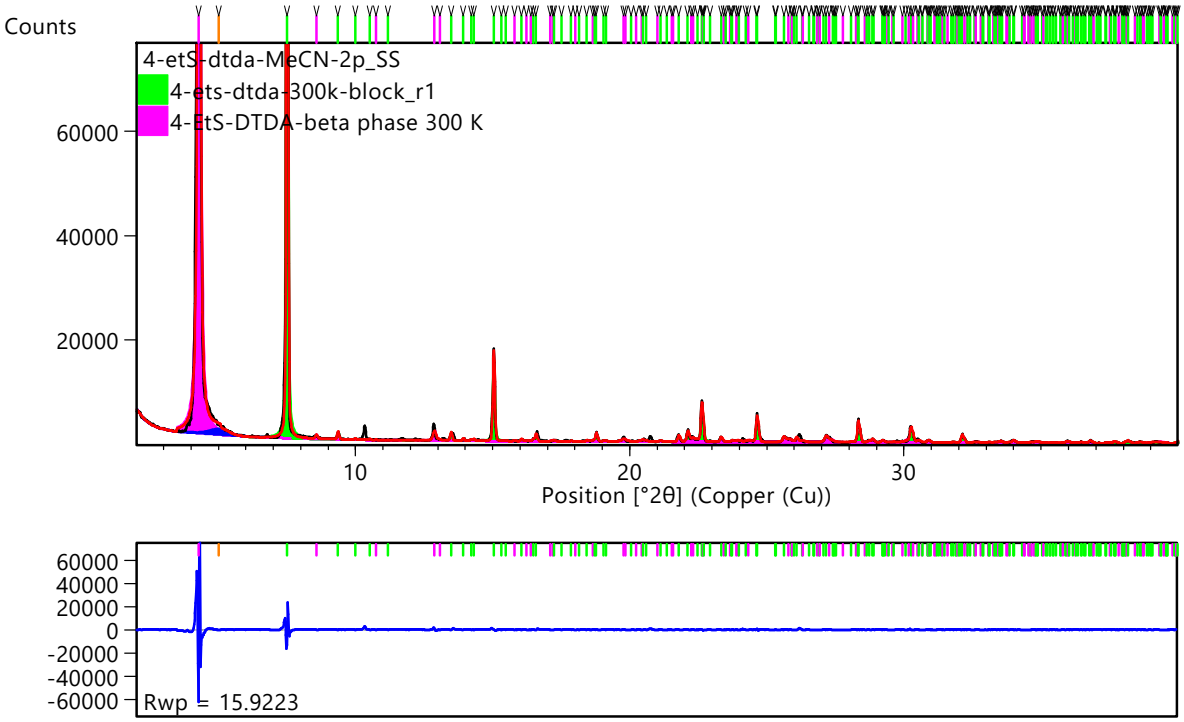

Figure S9. *Pawley refinement of the mixture of **3**α (green) and **3**β (fuschia) obtained by recrystallization of crude reduction mixture from MeCN. Experimental pattern is shown in black, refined profile in red, while green- and fuschia-colored markers on top correspond to characteristic Bragg peak positions of the assigned phases **3**α and **3**β, respectively. Difference plot of the experimental vs. refined profiles is shown below in blue. See Table S7.*

Table S7. Crystallographic data for **3** obtained by recrystallization from crude reaction mixture in MeCN.

Parameters	PXRD	PXRD	SC-XRD	SC-XRD
Temperature (K)	293	293	300	300
Phase	**3**α	**3**β	**3**α	**3**β
Crystal system	monoclinic	monoclinic	monoclinic	monoclinic
Space group	$P2_1/c$	*Pn*	$P2_1/c$	*Pn*
a /Å	12.6573(9)	5.767(2)	12.6651(3)	5.6566(2)
b /Å	15.809(1)	20.615(2)	15.7806(3)	20.2060(5)
c /Å	11.485(1)	9.235(3)	11.4706(3)	9.3436(3)
α /°	90	90	90	90
β /°	111.4810(9)	103.666(8)	111.534(3)	103.844(3)
γ /°	90	90	90	90
V/Å^3	2138.46	1066.81	2132.53(9)	1036.92(6)

$R_{prof.}$	0.1109
$R_{w\text{-}prof}$	0.1592
GOF	10.643

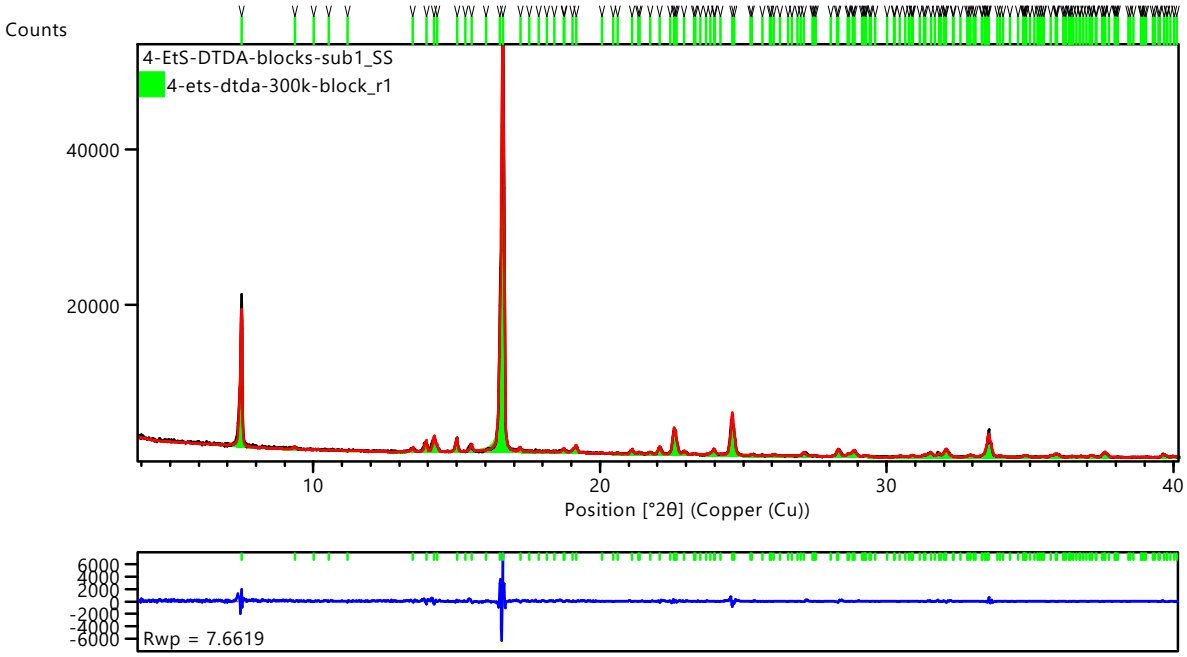

Figure S10. *Pawley refinement of **3**α from vacuum sublimation. Experimental pattern is shown in black, refined profile in red, while green-colored markers on top correspond to characteristic Bragg peak positions of the assigned **3**α phase. Difference plot of the experimental vs. refined profiles is shown below in blue. See Table S8.*

Table S8. Crystallographic data for **3**α from vacuum sublimation.

Parameters	PXRD	SC-XRD
Temperature (K)	293	300
Crystal system	monoclinic	monoclinic

Space group	$P2_1/c$	$P2_1/c$
a /Å	12.699(2)	12.6651(3)
b /Å	15.844(4)	15.7806(3)
c /Å	11.476(2)	11.4706(3)
α /°	90	90
β /°	111.461(2)	111.534(3)
γ /°	90	90
V/Å^3	2148.73	2132.53(9)
$R_{prof.}$	0.0609	
$R_{w\text{-}prof}$	0.0766	
GOF	2.417	

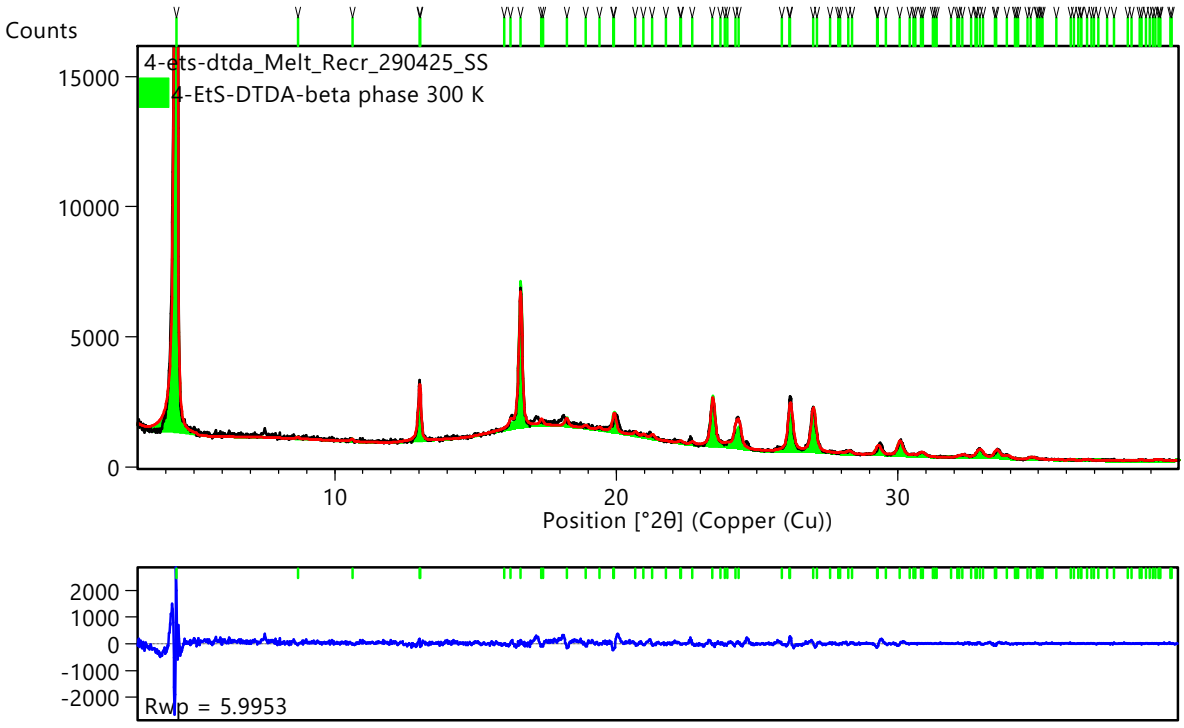

Figure S11. *Pawley refinement of **3**β by melt-recrystallization of **3** with slow cooling in an oil bath. Experimental pattern is shown in black, refined profile in red, while green-colored markers on top correspond to characteristic Bragg peak positions of the assigned **3**β phase. Difference plot of the experimental vs. refined profiles is shown below in blue. See Table S9.*

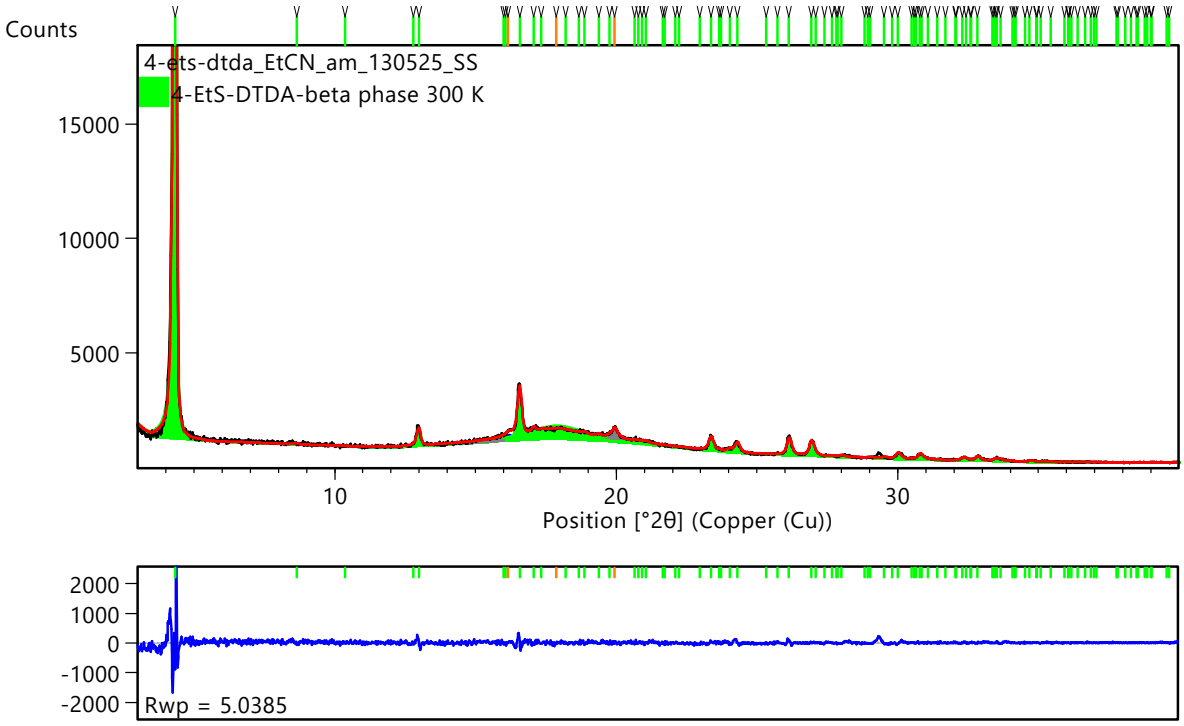

Figure S12. *Pawley refinement of **3**β from recrystallization of **3** in EtCN. Experimental pattern is shown in black, refined profile in red, while green-colored markers on top correspond to characteristic Bragg peak positions of the assigned **3**β phase. Difference plot of the experimental vs. refined profiles is shown below in blue. See Table S9.*

Table S9. Crystallographic data for **3**β.

Parameters	PXRD	PXRD	SC-XRD
Temperature (K)	293	293	300
Obtained from	melt-recrystallization	recrystallization EtCN	recrystallization EtCN
Crystal system	monoclinic	monoclinic	monoclinic
Space group	*Pn*	*Pn*	*Pn*
a /Å	5.690(2)	5.710(3)	5.6566(2)
b /Å	20.45(1)	20.46(1)	20.2060(5)
c /Å	9.407(3)	9.683(6)	9.3436(3)
α /°	90	90	90
β /°	102.846(4)	103.842(5)	103.844(3)
γ /°	90	90	90
V/Å^3	1067.26	1098.23	1036.92(6)
$R_{prof.}$	0.0508	0.0401	
$R_{w\text{-}prof}$	0.0599	0.0503	
GOF	1.690	1.322	

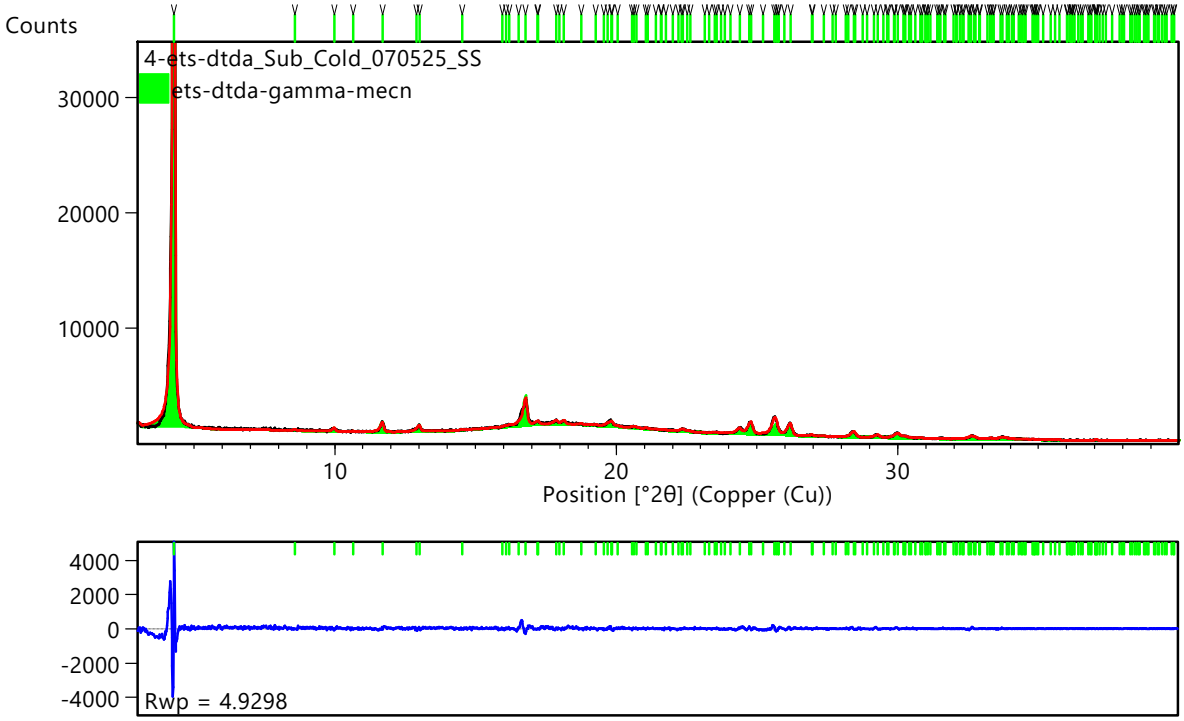

Figure S13. *Pawley refinement of* ***3****γ from vacuum sublimation. Experimental pattern is shown in black, refined profile in red, while green-colored markers on top correspond to characteristic Bragg peak positions of the assigned* ***3****γ phase. Difference plot of the experimental vs. refined profiles is shown below in blue. See Table S10.*

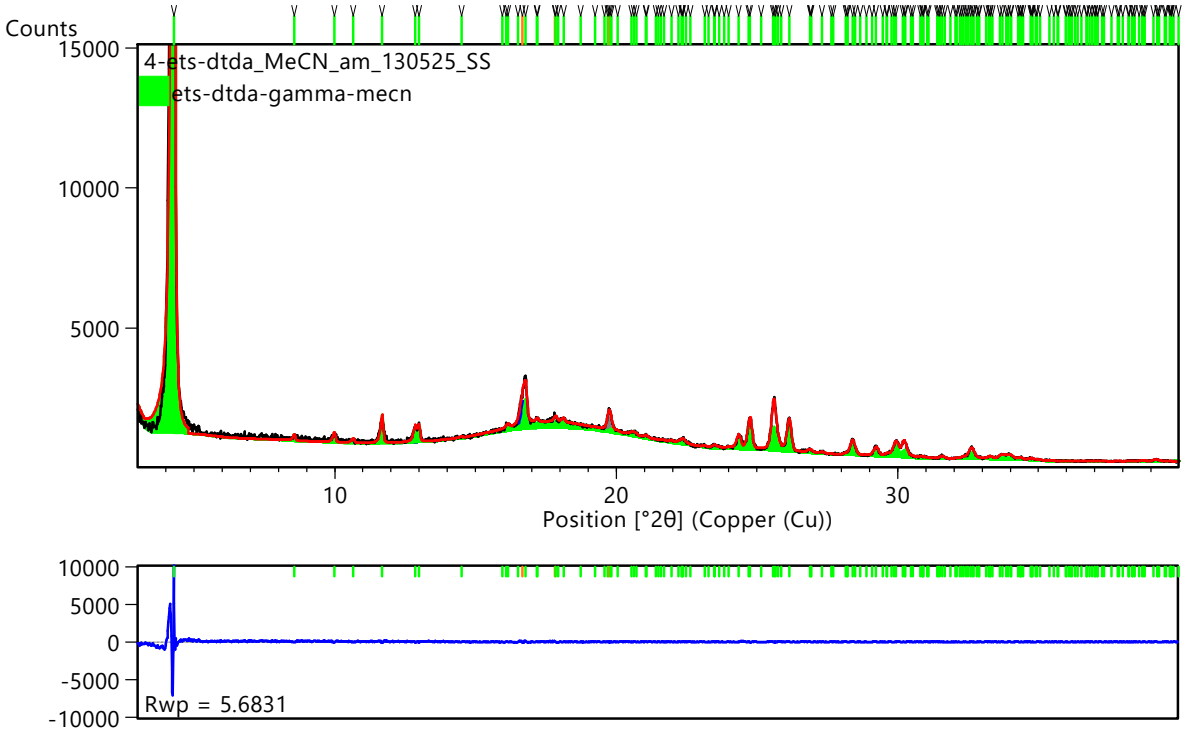

Figure S14. *Pawley refinement of **3**γ from recrystallization of **3** in MeCN. Experimental pattern is shown in black, refined profile in red, while green-colored markers on top correspond to characteristic Bragg peak positions of the assigned **3**γ phase. Difference plot of the experimental vs. refined profiles is shown below in blue. See Table S10.*

Table S10. Crystallographic data for **3**γ.

Parameters	PXRD	PXRD	SC-XRD
Temperature (K)	293	293	300
Obtained from	sublimation	recrystallization MeCN	sublimation
Crystal system	monoclinic	monoclinic	monoclinic
Space group	$P2_1/n$	$P2_1/n$	$P2_1/n$
a /Å	5.711(4)	5.717(4)	5.7190(3)
b /Å	41.14(4)	41.32(4)	41.353(3)
c /Å	9.325(6)	9.329(7)	9.3267(4)
α /°	90	90	90
β /°	103.523(5)	103.521(6)	103.8020(10)
γ /°	90	90	90
V/Å^3	2152.02	2142.45	2124.47(2)
$R_{prof.}$	0.0469	0.0544	
$R_{w\text{-}prof}$	0.0493	0.0568	
GOF	1.447	1.631	

Note. Reviewer comments highlighted a small apparent negative thermal expansion (NTE) in the **3**-polymorph series. We believe this effect is most pronounced along the herringbone stacking direction as indicated in Tables S8-S10. The molecular conformation and packing of the **3** series make its crystals more compliant, where the gentle grinding required for PXRD sample preparation likely introduces anisotropic strain that is preferentially released throughout the herringbone layers allowing it to relax into a more efficient packing and manifesting as an overall increase in the unit cell volume of ~ 30–60 Å^3. In contrast, compounds **1**, **2**, **4**, **5** and **6** possess more rigid, interpenetrated structures making them resistant to deformation during grinding, thus exhibiting normal positive thermal expansion. This inherent rigidity also accounts for their lack of polymorphism. We acknowledge that inherent limitations to the PXRD-derived cells may also contribute to these subtle volume differences. Further analysis of the crystal packing motifs is provided in Section 7.

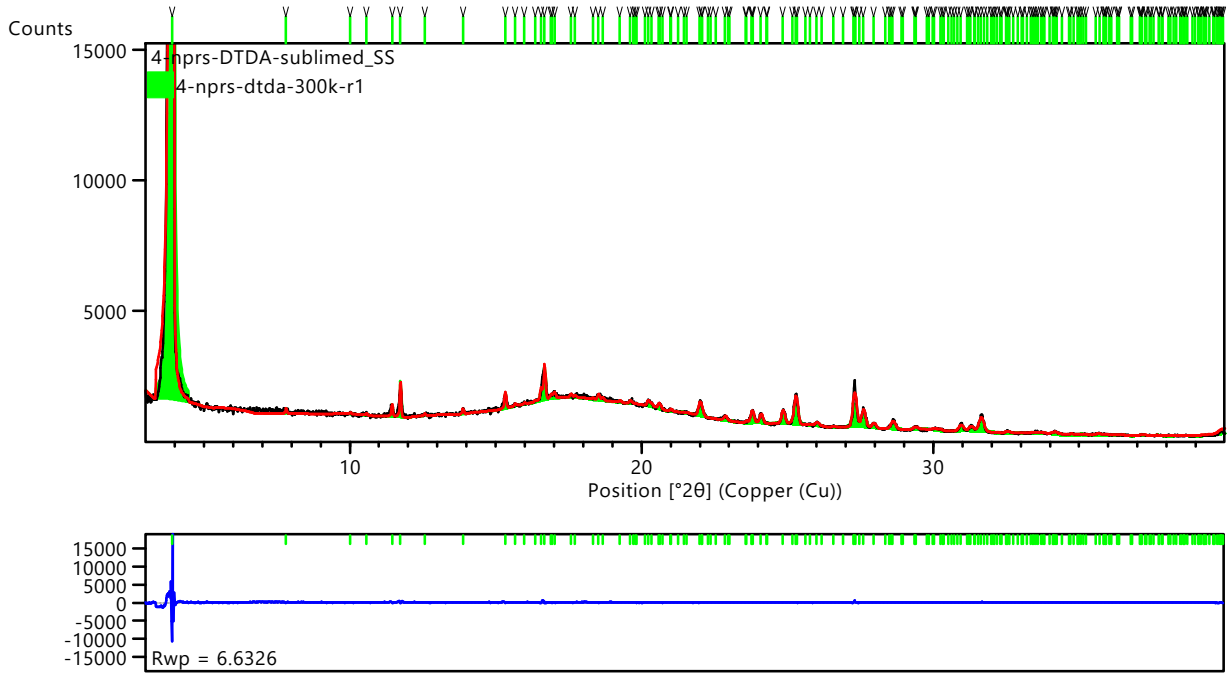

Figure S15. *Pawley refinement of **4** from vacuum sublimation. Experimental pattern is shown in black, refined profile in red, while green-colored markers on top correspond to characteristic Bragg peak positions of the assigned phase. Difference plot of the experimental vs. refined profiles is shown below in blue. See Table S11.*

Table S11. Crystallographic data for **4** from vacuum sublimation.

Parameters	PXRD	SC-XRD
Temperature (K)	293	300
Crystal system	monoclinic	monoclinic
Space group	$P2_1/n$	$P2_1/n$
a /Å	5.750(1)	5.75410(10)
b /Å	45.23(1)	45.2695(5)
c /Å	9.267(2)	9.2598(2)
α /°	90	90
β /°	103.857(3)	103.684(2)
γ /°	90	90
V/Å^3	2339.70	2343.58(7)
$R_{prof.}$	0.0540	90
$R_{w\text{-}prof}$	0.0663	

GOF	1.904

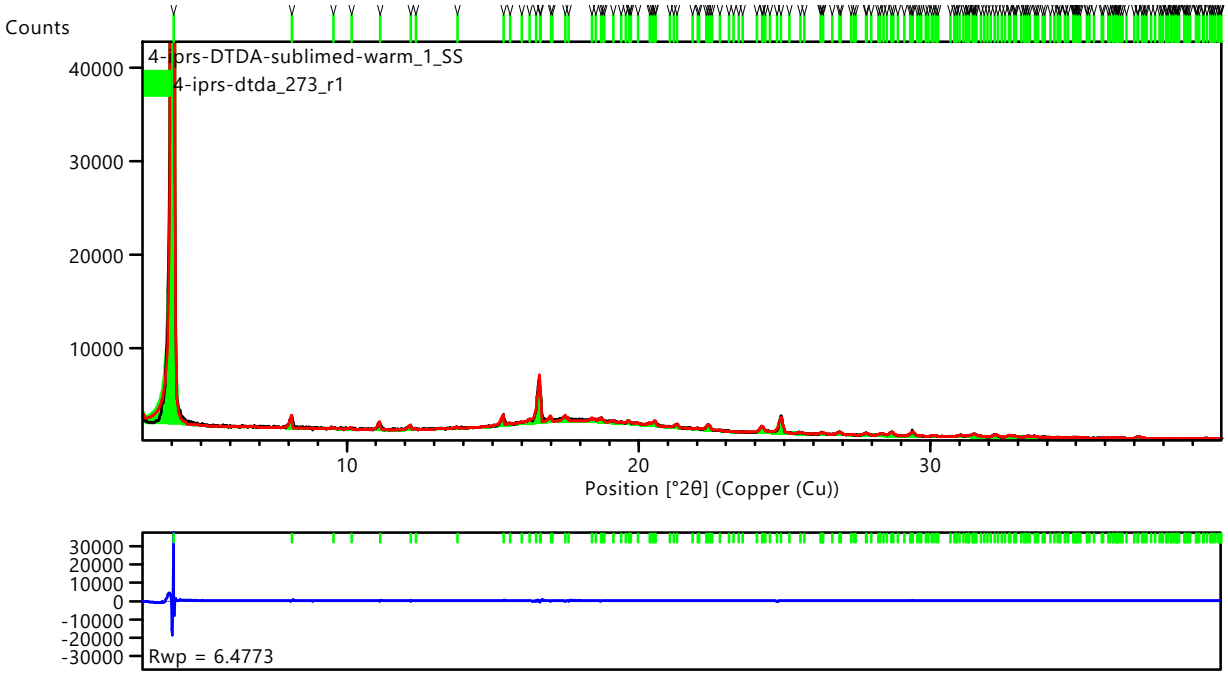

Figure S16. *Pawley refinement of* ***5*** *from vacuum sublimation. Experimental pattern is shown in black, refined profile in red, while green-colored markers on top correspond to characteristic Bragg peak positions of the assigned phase. Difference plot of the experimental vs. refined profiles is shown below in blue. See Table S12.*

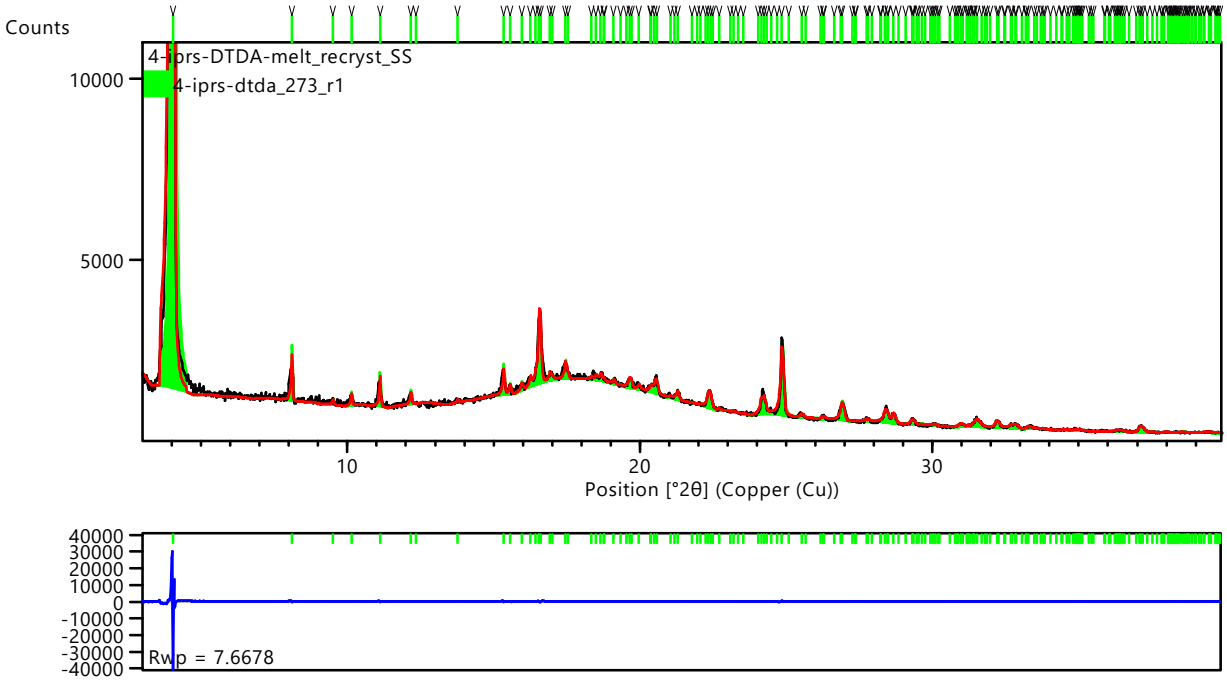

Figure S17. *Pawley refinement of* ***5*** *from melt-recrystallization. Experimental pattern is shown in black, refined profile in red, while green-colored markers on top correspond to characteristic Bragg peak positions of the assigned phase. Difference plot of the experimental vs. refined profiles is shown below in blue. See Table S12.*

Table S12. Crystallographic data for **5**.

Parameters	PXRD	PXRD	SC-XRD
Temperature (K)	293	293	273
Obtained from	sublimation	melt-recrystallization	sublimation
Crystal system	monoclinic	monoclinic	monoclinic
Space group	$P2_1/c$	$P2_1/c$	$P2_1/c$
a /Å	5.832(1)	5.842(2)	5.8238(2)
b /Å	43.569(4)	43.55(1)	43.3605(6)
c /Å	12.194(3)	12.231(4)	12.1776(4)
α /°	90	90	90
β /°	128.931(3)	129.064(5)	128.977(5)
γ /°	90	90	90
V/Å^3	2410.31	2415.97	2390.59(18)
$R_{prof.}$	0.0606	0.0772	
$R_{w\text{-}prof}$	0.0645	0.0767	
GOF	2.257	2.222	

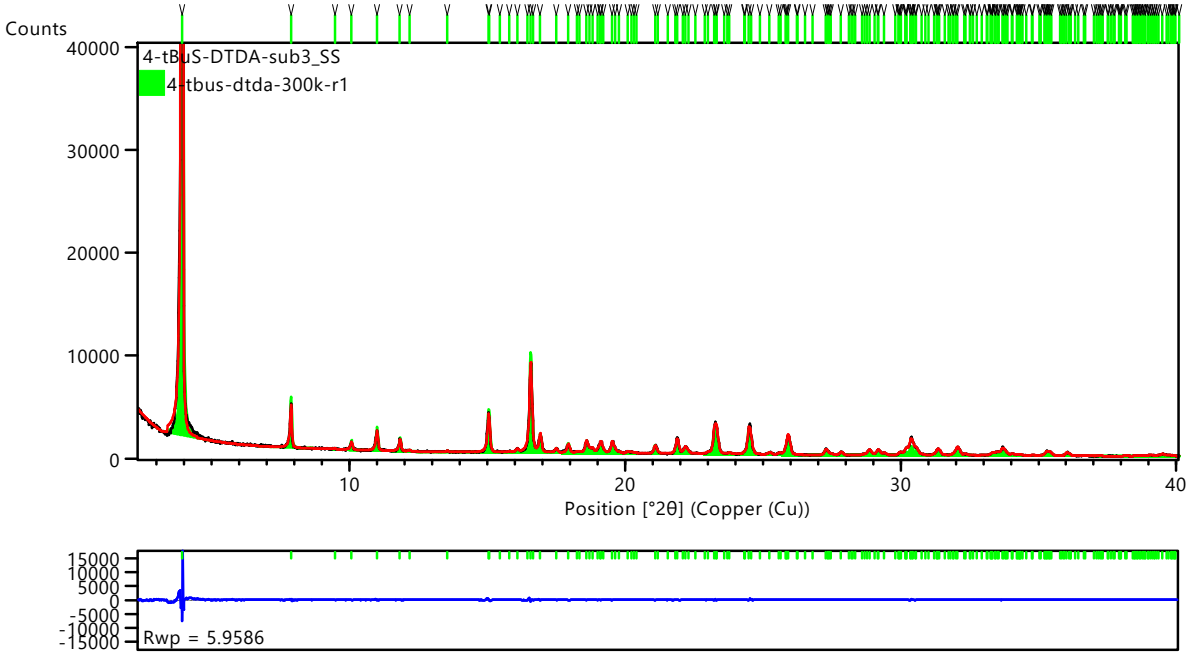

Figure S18. *Pawley refinement of* ***6*** *from vacuum sublimation. Experimental pattern is shown in black, refined profile in red, while green-colored markers on top correspond to characteristic Bragg peak positions of the assigned phase. Difference plot of the experimental vs. refined profiles is shown below in blue. See Table S13.*

Table S13. Crystallographic data for **6** from vacuum sublimation.

Parameters	PXRD	SC-XRD
Temperature (K)	293	300
Crystal system	monoclinic	monoclinic
Space group	$P2_1/n$	$P2_1/n$
a /Å	5.9823(6)	5.98820(10)
b /Å	44.847(6)	44.9141(9)
c /Å	9.632(1)	9.6438(2)
α /°	90	90
β /°	98.127(2)	97.849(2)
γ /°	90	90
V/Å^3	2558.17	2569.44(9)
$R_{prof.}$	0.0569	
$R_{w\text{-}prof}$	0.0596	
GOF	1.590	

4 Thermal Studies

4.1 Thermogravimetric Analysis (TGA)

Thermogravimetric analysis (TGA) was performed on a PerkinElmer STA 600 simultaneous thermal (TG/DSC) analyzer using an open platinum pan under nitrogen atmosphere (flow rate 40 mL min^{-1}) with a heating rate of 10 K min^{-1}. Temperature calibration was done with an indium standard and weight calibration by a standard weight of 50 mg. All samples were freshly prepared and dried *in vacuo* prior to measurement where 3–8 mg was typically used. Recorded TG data were processed using the Pyris Manager software (v. 13).

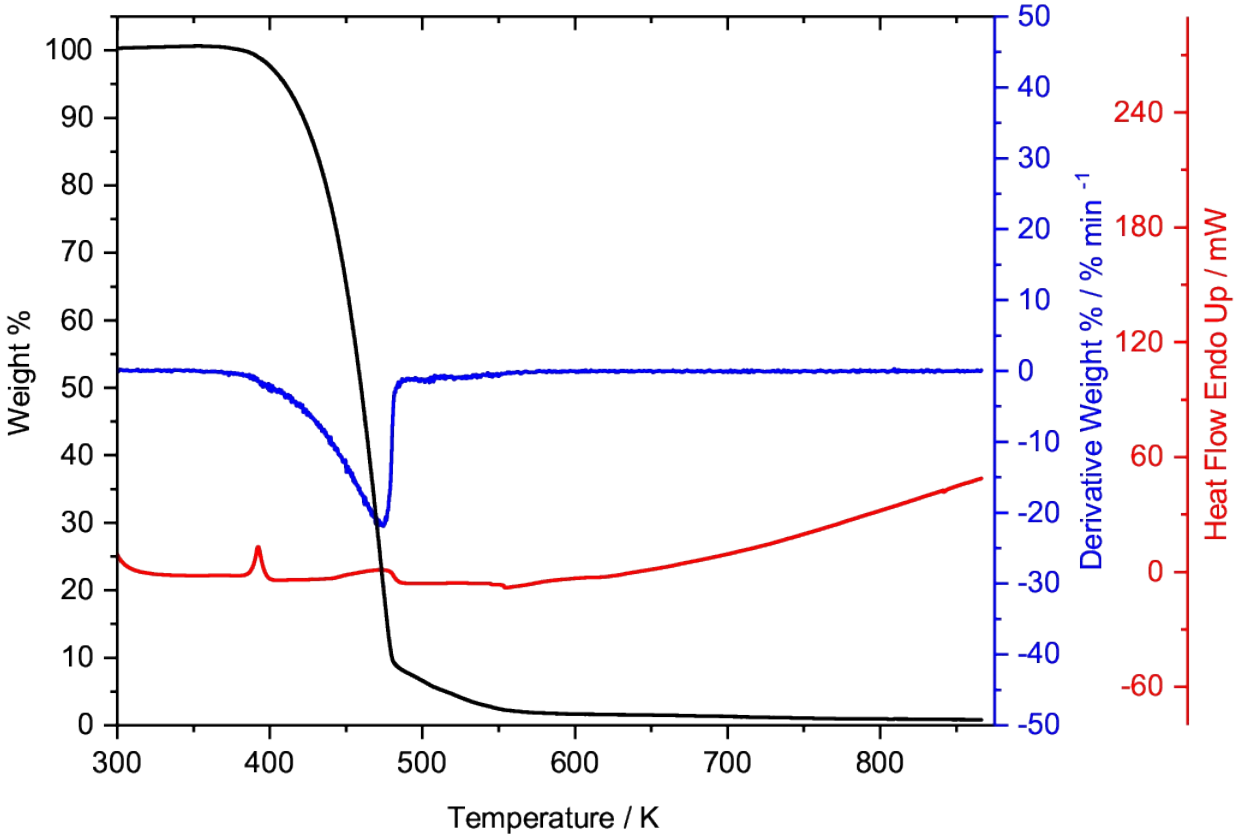

Figure S19. *TGA of* ***1*** *recorded between 300 to 875 K.*

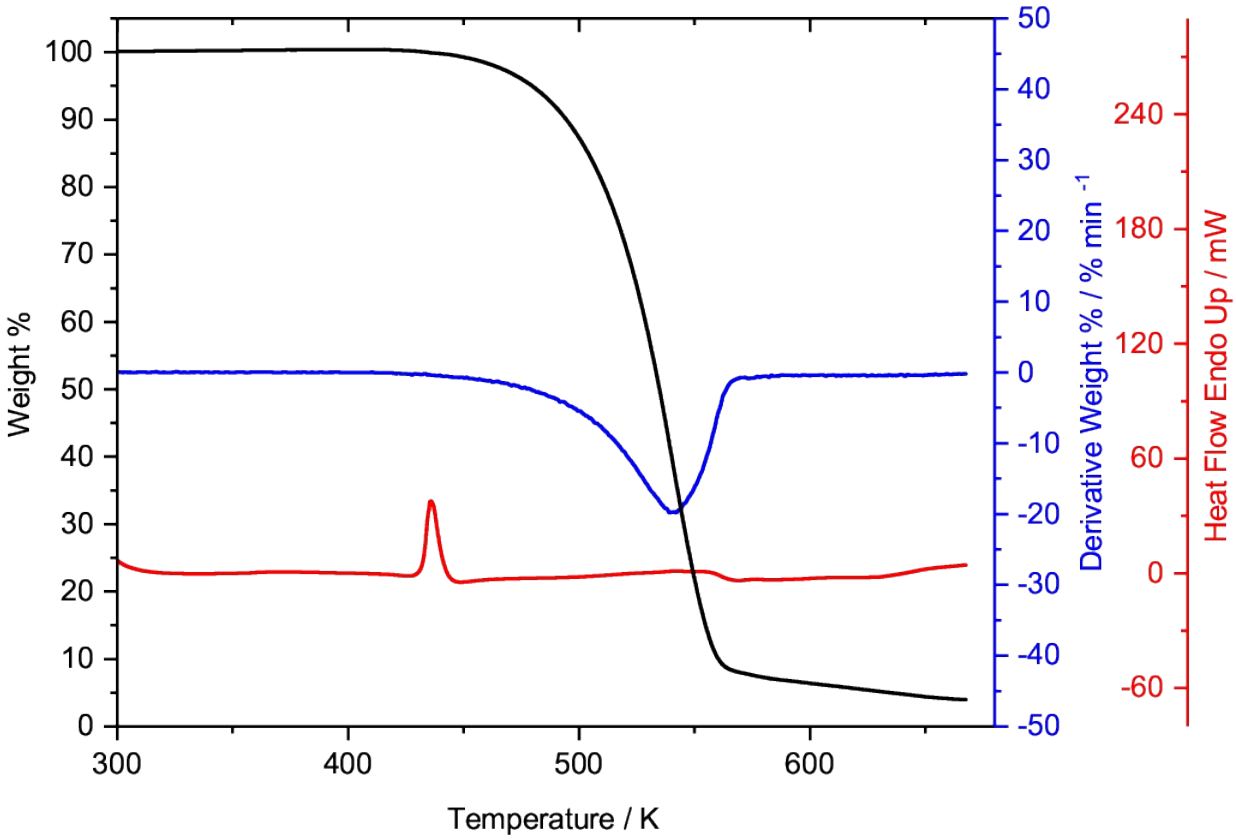

Figure S20. *TGA of* ***2*** *recorded between 300 to 675 K.*

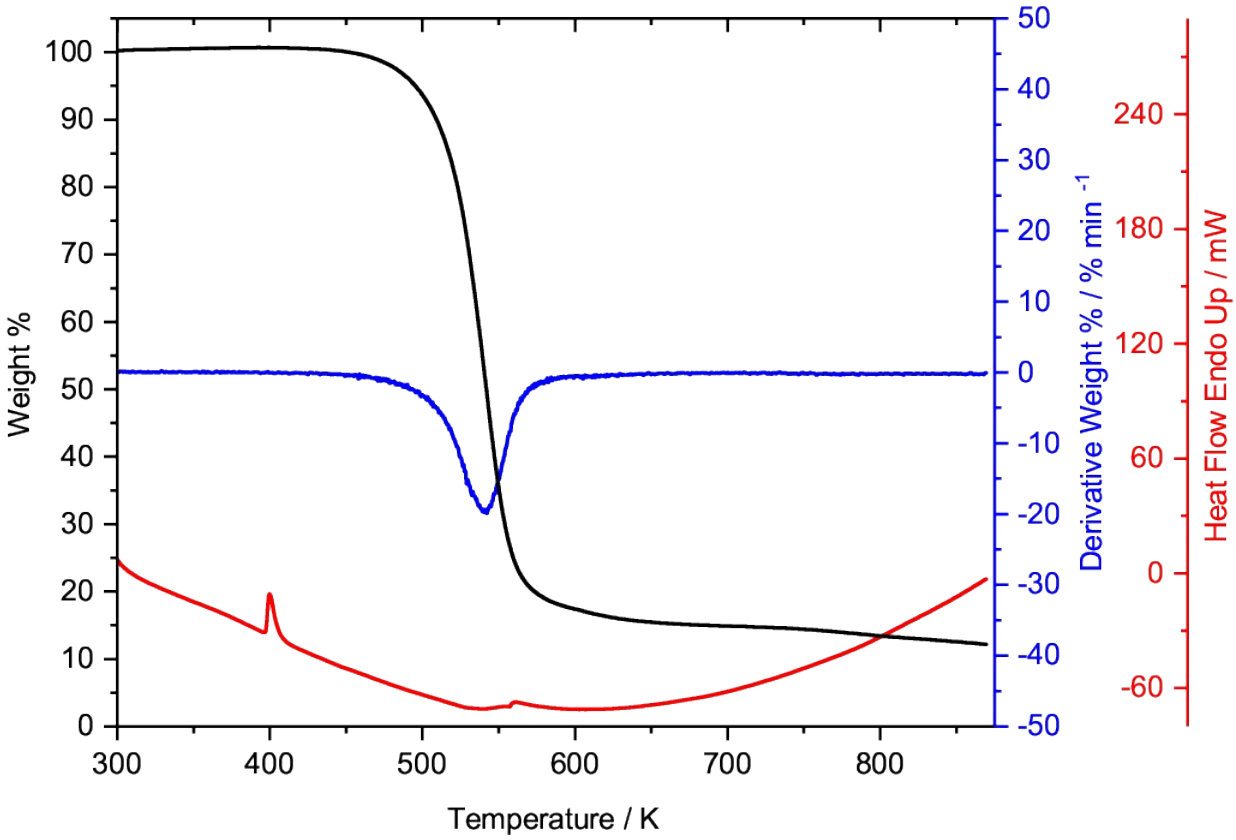

Figure S21. *TGA of* ***3****α recorded between 300 to 875 K.*

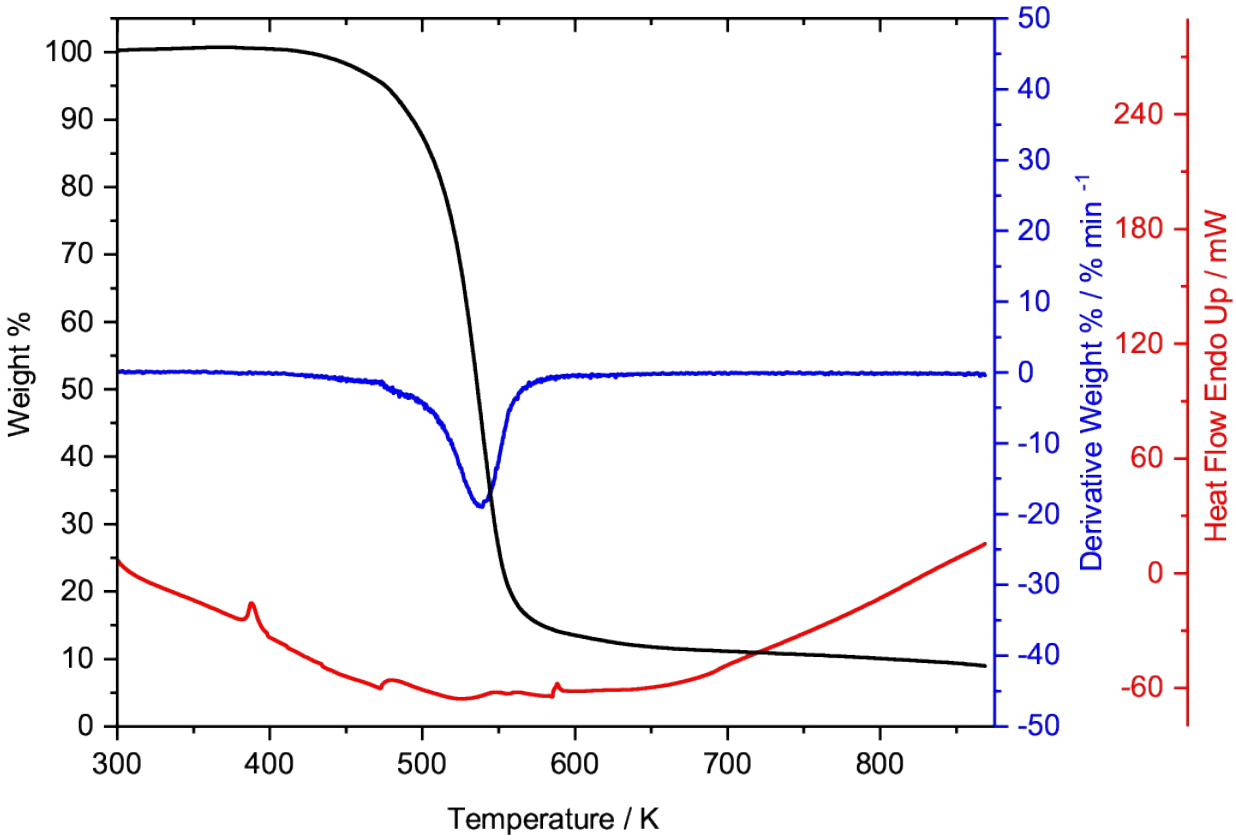

Figure S22. *TGA of* ***4*** *recorded between 300 to 875 K.*

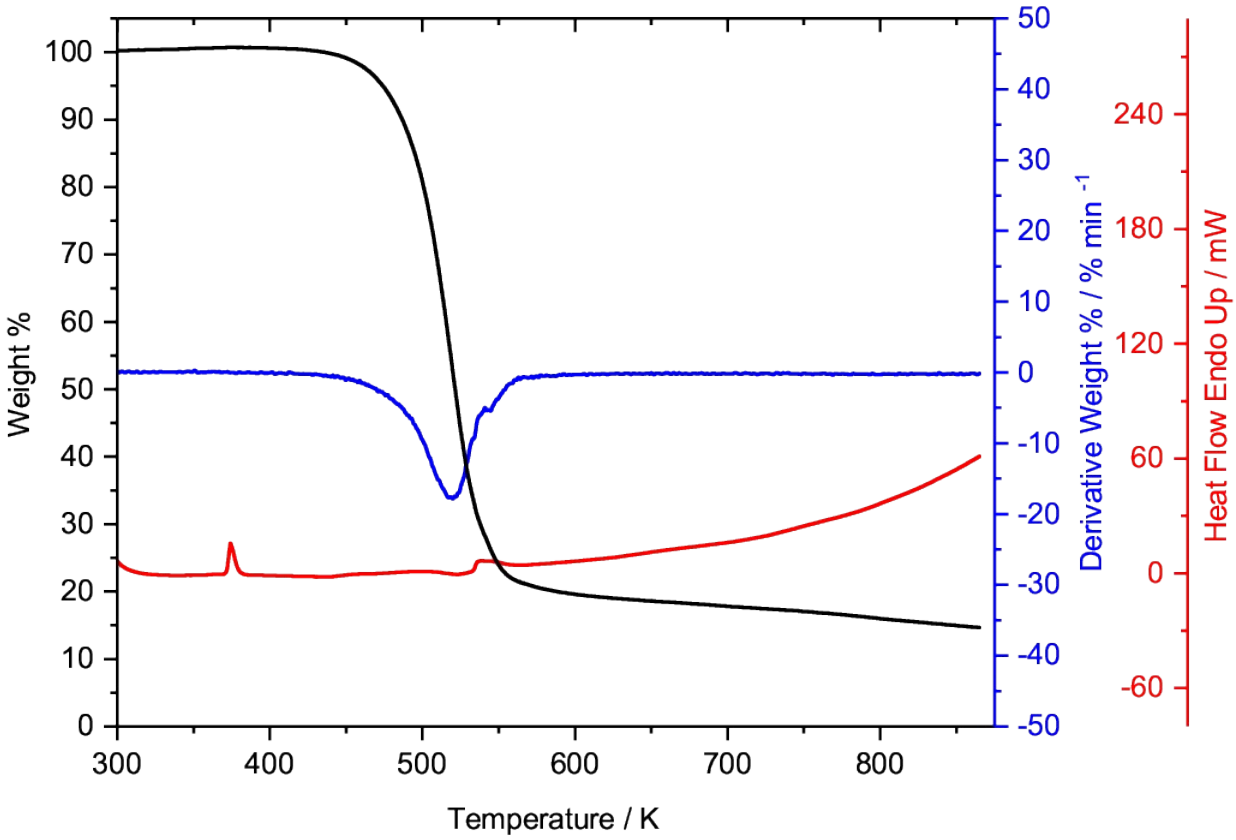

Figure S23. *TGA of* ***5*** *recorded between 300 to 875 K.*

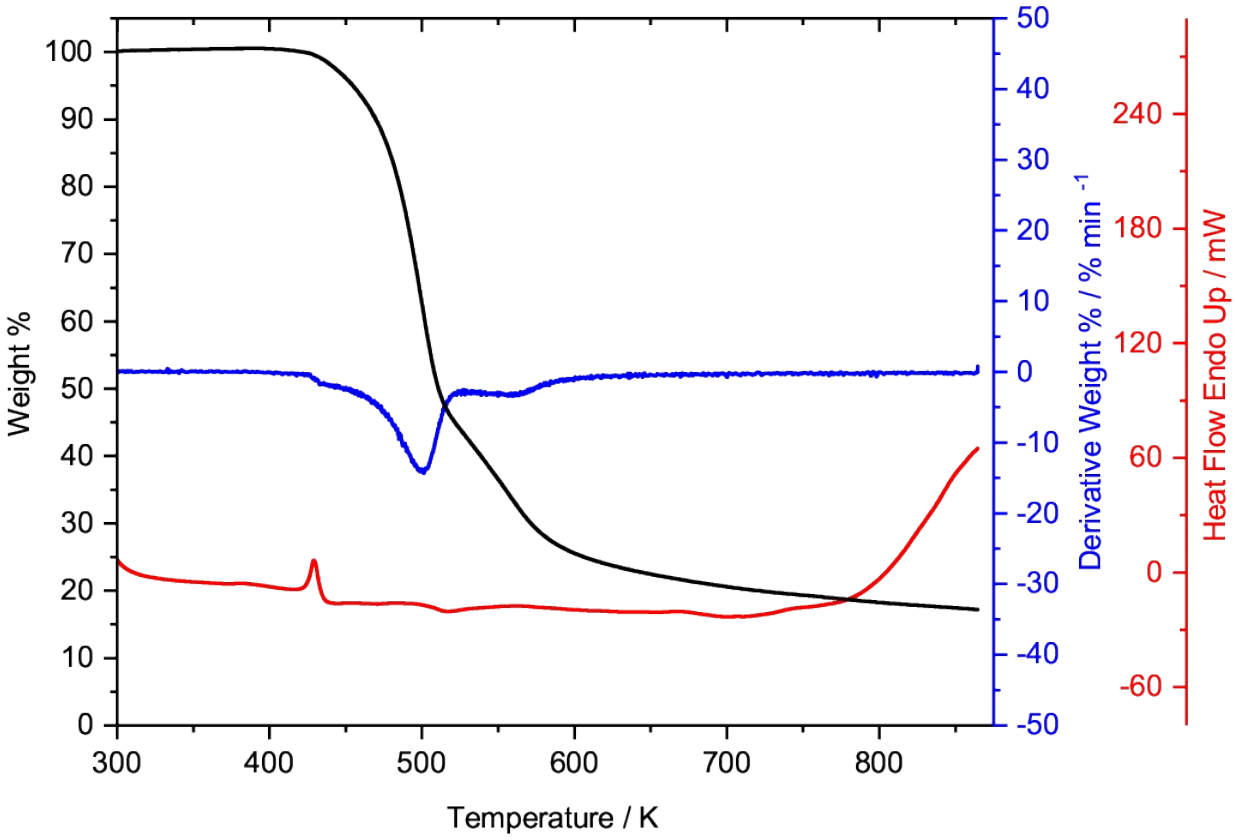

Figure S24. *TGA of* ***6*** *recorded between 300 to 875 K.*

Table S14. Approximate onset values determined by TGA

Compound	Melt / K	Sublimation / K
1	388	392
2	433	457
3α	397	465
4	384	440
5	372	447
6	423	428

4.2 Differential Scanning Calorimetry (DSC)

Differential scanning calorimetry (DSC) data were obtained using a power compensation type PerkinElmer DSC 8500 series instrument and a hermetically sealed 50 µL aluminum pan prepared

under an atmosphere of argon. All heating and cooling scans were done under nitrogen (flow rate 50 mL min^{-1}) with typical scanning rates of 2–10 K min^{-1}. The instrument was calibrated using two temperature standards (*n*-decane and indium), and one energy standard (indium). See Table 3 for averaged onset values determined by DSC.

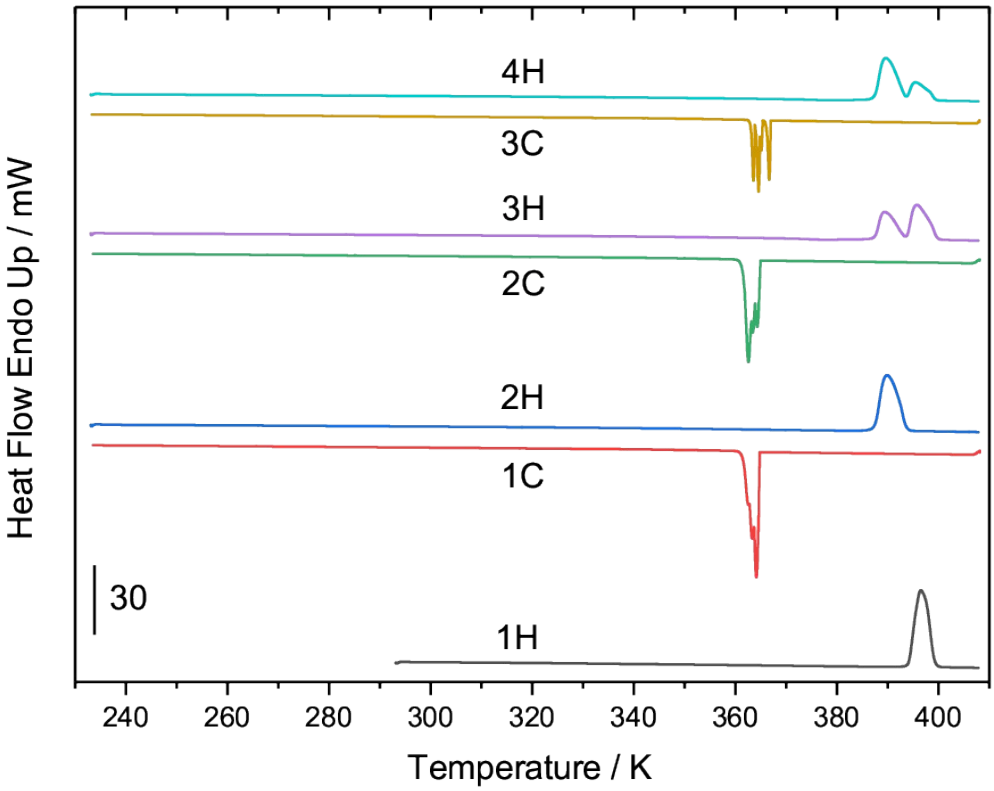

Figure S25. *DSC curves of* ***3****α (4.466 mg) at 10 K* min^{-1}*. The labels denote the number of the heating (H) or cooling (C) cycle.*

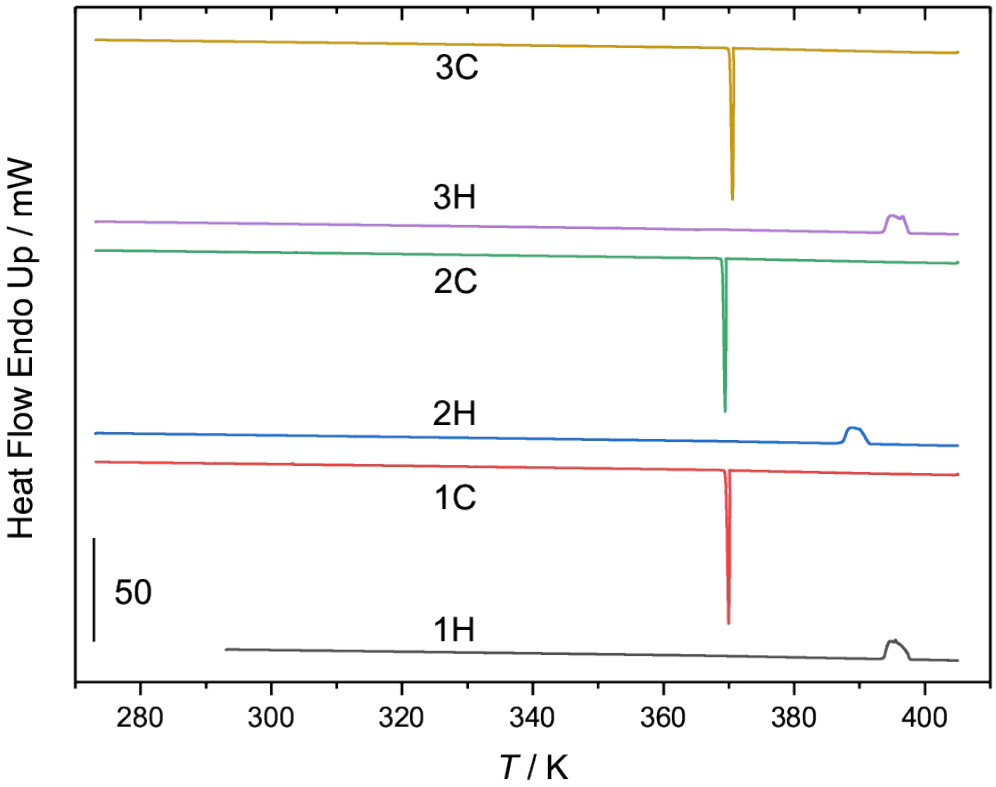

Figure S26. *DSC curves of **3**α (5.313 mg) at 2 K min^{-1}. The labels denote the number of the heating (H) or cooling (C) cycle. Onsets of melting at ~394 K (1H, 3H) and at ~388 K (2H) possibly due to the interplay of two crystal phases with different melting points. Enthalpies of fusion (cf. Table S15) calculated from the area of the respective endotherms: 1H (140 J g^{-1}), 2H (131 J g^{-1}), 3H (140 J g^{-1}).*

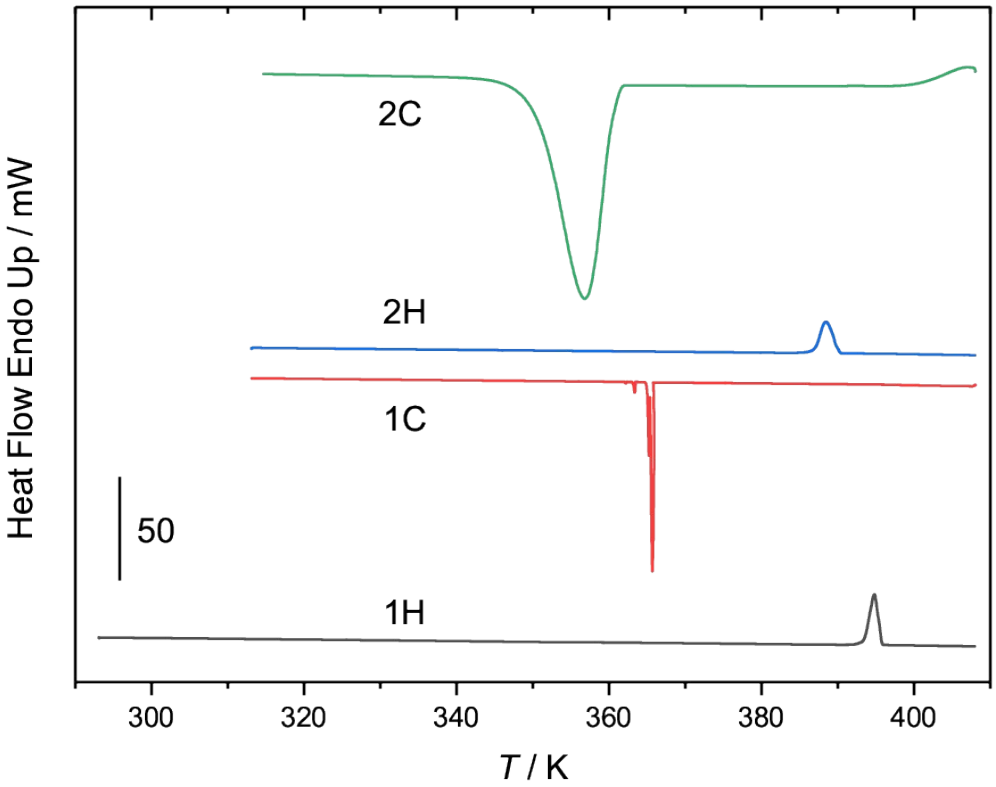

Figure S27. *DSC curves of* ***3****β (7.050 mg) at 2 K min^{-1} (50 K min^{-1} on 2C).*

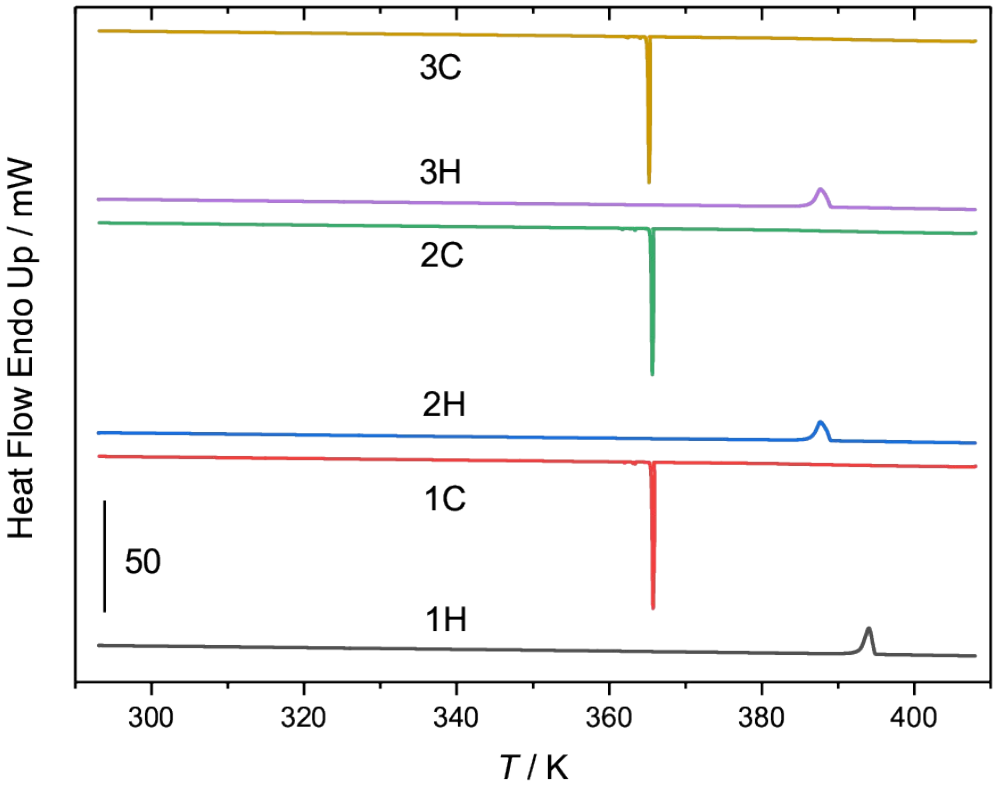

Figure S28. *DSC curves of **3**γ (3.505 mg) at 2 K min^{-1}. The labels denote the number of the heating (H) or cooling (C) cycle. Onsets of melting at ~393K (1H) and at ~386 K (2H, 3H). Enthalpies of fusion (cf. Table S15) calculated from the area of the respective endotherms: 1H (138 J g^{-1}), 2H (135 J g^{-1}), 3H (136 J g^{-1}).*

Table S15. Enthalpies of fusion ($\Delta H_{fus.}$) and solidification ($\Delta H_{sol.}$) calculated from the areas of the respective endo- and exotherms on DSC heating (H) and cooling (C) cycles at 10 K min^{-1}, in J g^{-1}.

	1H	1C	2H	2C	3H
	$\Delta H_{sol.}$	$\Delta H_{fus.}$	$\Delta H_{sol.}$	$\Delta H_{fus.}$	$\Delta H_{sol.}$
1	143.93	-136.30	143.29	-136.24	
2	165.34	-156.52	164.54	-156.46	164.13
3α	142.58	-119.05	130.91	-118.57	136.22
4	112.17	-100.96	111.50	-101.21	111.13
5	95.83	-87.47	95.33	-88.07	95.08
6	137.75	-127.30	128.47	-123.68	122.58

4.3 Hot-stage Microscopy

Hot-stage microscopy was performed on an Olympus BX51 microscope with a U-LH100-3 light source, on a Linkam T95-HS temperature-controlled stage under nitrogen flow. Images were captured on an Olympus DP23 digital camera mounted with a U-TV1XC adapter. The samples were prepared inside a glove box and sealed between a microscope and cover slide using silicone grease. Brightness of the images has been adjusted for clarity.

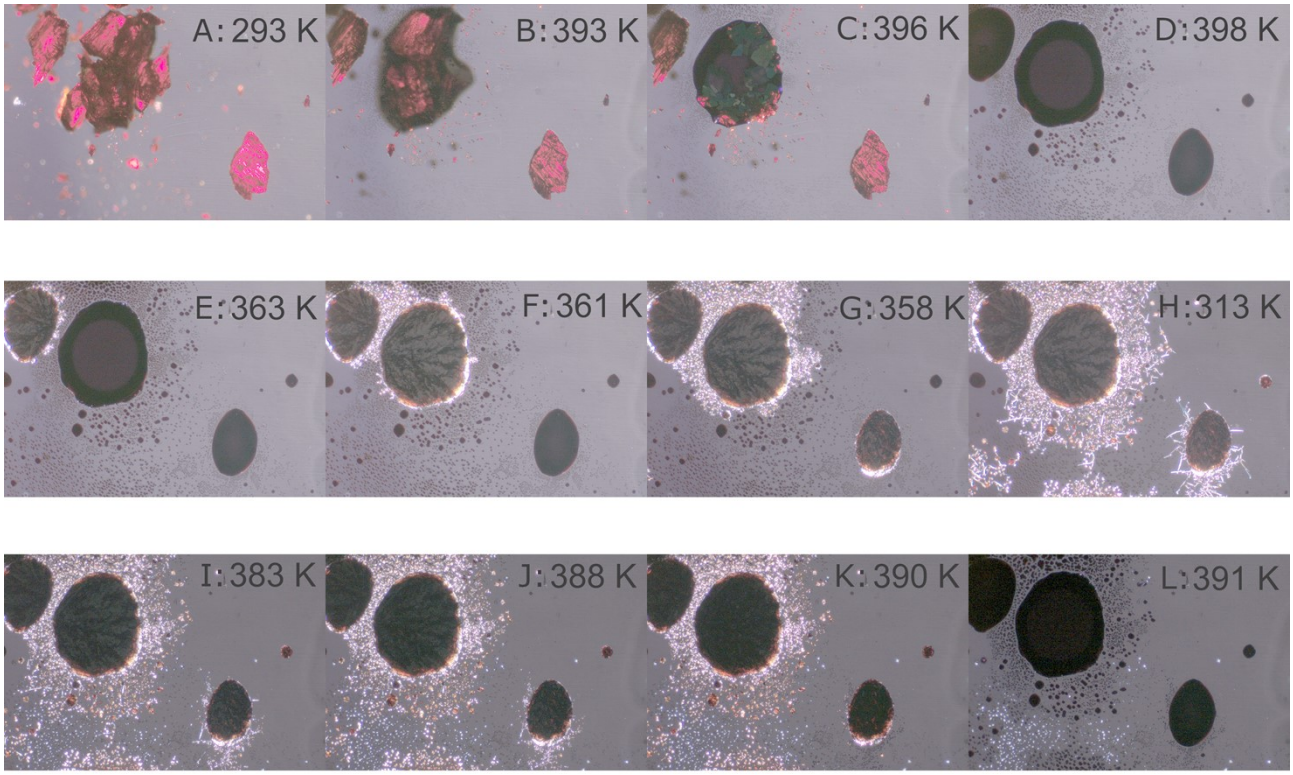

Figure S29. *Hot-stage microscopy of a mixture of* ***3****α and* ***3****γ (A), with select crystals displaying a solid-liquid-solid transition (B,C) followed by melting (D). On cooling, recrystallization begins at 363 K (E), and quickly propagates (F,G), while further cooling reveals the formation of needles (H). On repeated heating, the melting begins more gradually with the needles disappearing first (I-K), while the bulk rapidly melts afterwards (L), considerably earlier compared to both melting events seen during the first heating cycle.*

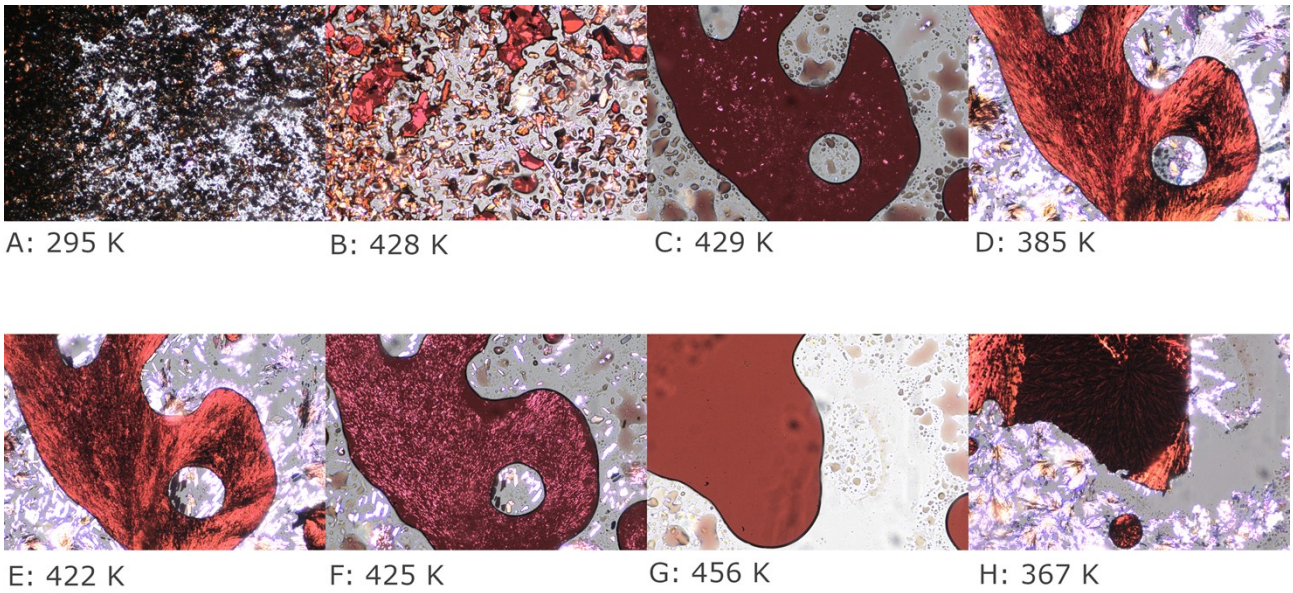

Figure S30. *Hot-stage microscopy of* ***6*** *at 10 K min^{-1} heating and cooling, beginning from neat crystals (A), displaying melting of bulk material (B), followed by recrystallization (D). Second heating cycle displaying melting (F,G) and cooling cycle showing recrystallization (H).*

5 Magnetic Studies

The variable temperature magnetic susceptibility measurements were performed on a vibrating sample magnetometer (VSM) under an applied field of 1 T. The choice of a 1 T magnetic field for susceptibility measurements was motivated by the need to achieve a robust signal-to-noise ratio, particularly given the weak magnetic response of the organic radicals in our sample (especially at room temperature). While lower fields are often employed in conventional susceptibility measurements, the inherently small magnetic moment of our system necessitated a higher field to ensure reliable detection of the paramagnetic signal but the present conditions were carefully optimized to balance sensitivity and experimental feasibility.

The samples (18.4 mg for **1**, 19.8 mg for **2**, 21.5 mg for **3**α, 25.4 mg for **4**, 20.2 mg for **5** and 23.0 mg for **6**) were loaded either into (a) quartz tubes (~3 mm I.D.) that were sealed a 3 mm quartz or Pyrex rod and epoxy or (b) high-purity silver capsules (2 x 5 x 0.1 mm) that were mechanically

sealed and attached to Pyrex rods with epoxy and Teflon tape. All samples were prepared in an argon filled glovebox. The experimental data were corrected for the diamagnetic contribution of the sample holder and of the ligands based on Pascal's constants. Measurements were conducted from ambient temperature using heating/cooling rates 2, 5, and 10 K min^{-1}.

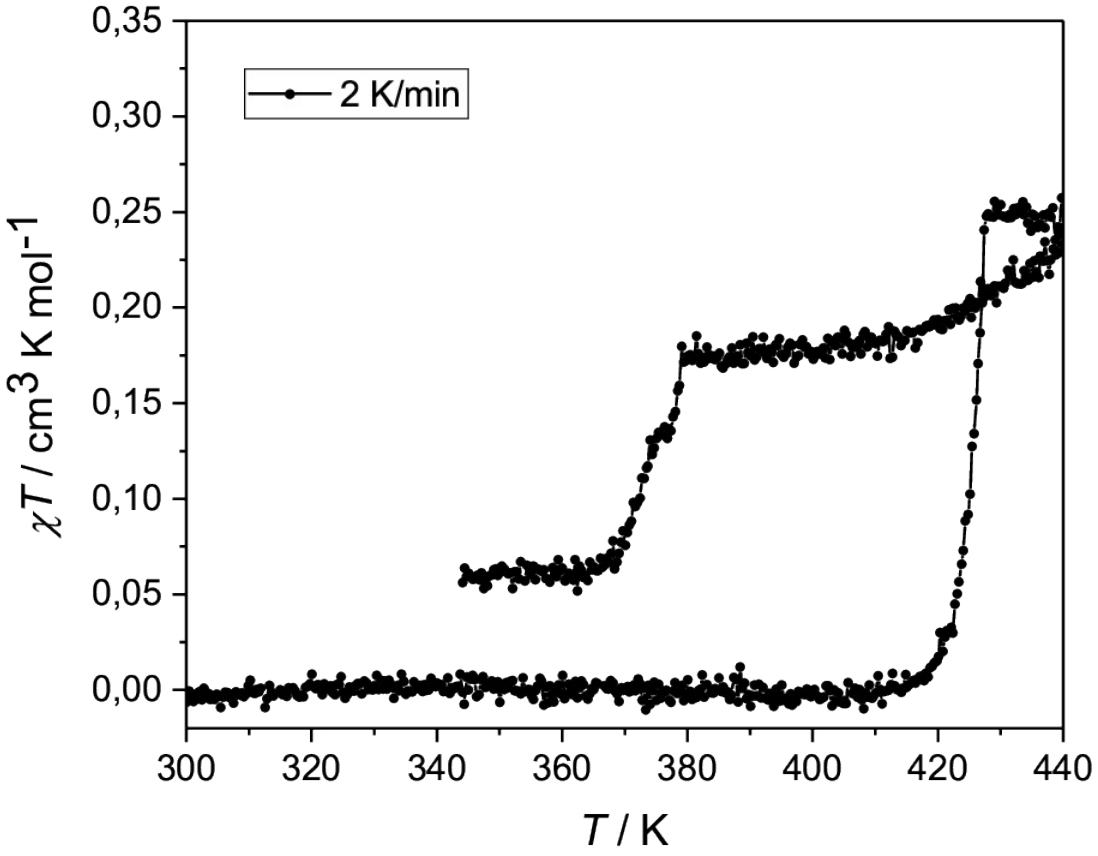

Figure S31*. Plot of the χT vs T of* ***6*** *measured at 2 K min-1 displaying a loss of centering above 420 K because of sample volatility and shifting baseline caused by loss of sample from sample holder.*

6 Computational Studies

Electrostatic potential (ESP) surfaces were calculated using Gaussian 16.[8] The asymmetric units from **1**–**6** were extracted from the room-temperature crystal structures, and the positions of hydrogens were optimized at the PBE0 / def2-TZVP + GD3BJ level.[9,10] The ESPs were subsequently plotted with GaussView (*vide infra*). Alternatively, the ESPs were mapped onto Hirshfeld[11] surfaces plotted

in CrystalExplorer21.5[12] using the default Tonto program for wave function calculation at the HF / STO-3G level. 2D fingerprints of the Hirshfeld surfaces were generated in CrystalExplorer21.5.

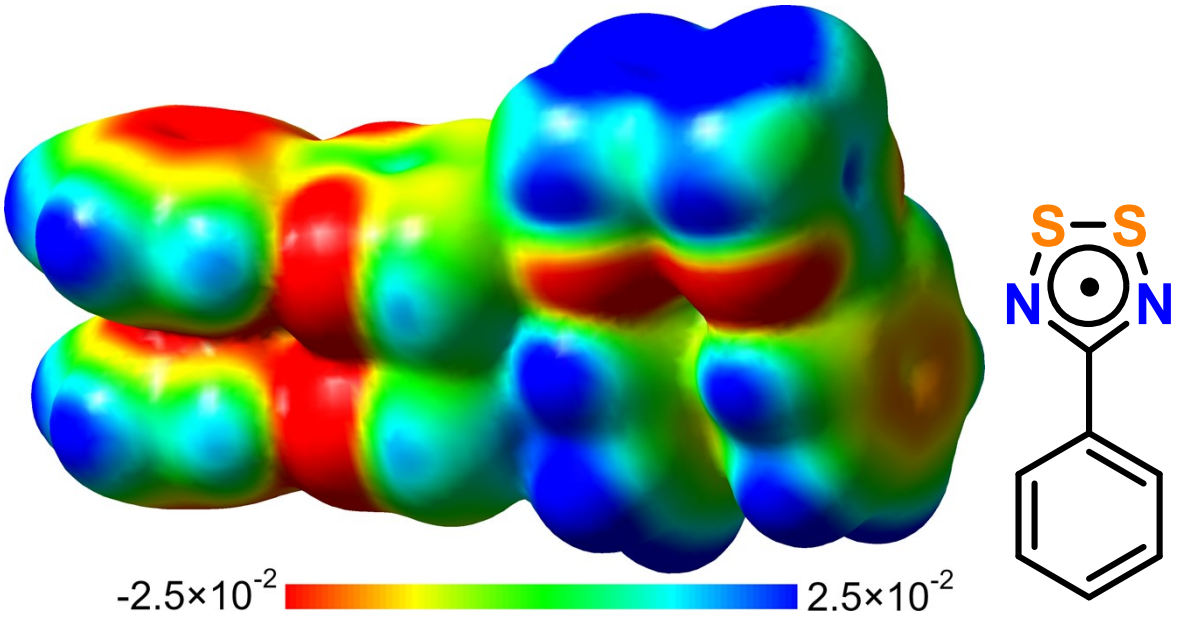

Figure S32. *Electrostatic potential mapped onto the asymmetric unit of* ***1*** *at electron density isovalue of 0.002 atomic units.*

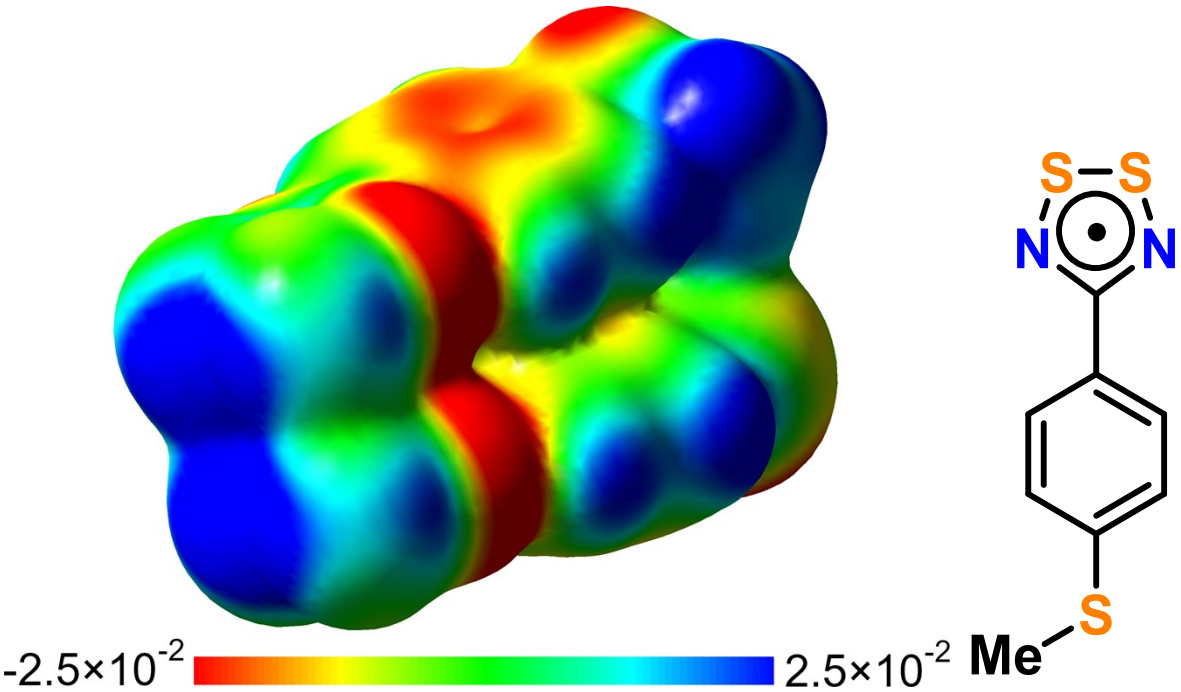

Figure S33. *Electrostatic potential mapped onto the asymmetric unit of* ***2*** *at electron density isovalue of 0.002 atomic units.*

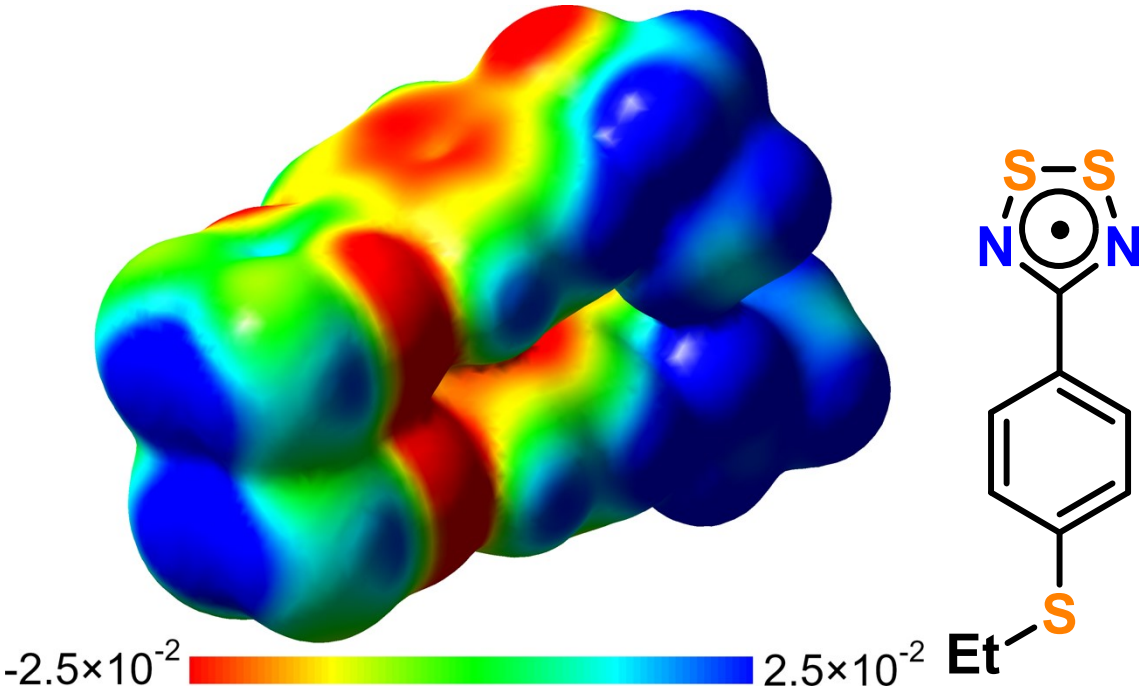

Figure S34. *Electrostatic potential mapped onto the asymmetric unit of* ***3****α at electron density isovalue of 0.002 atomic units.*

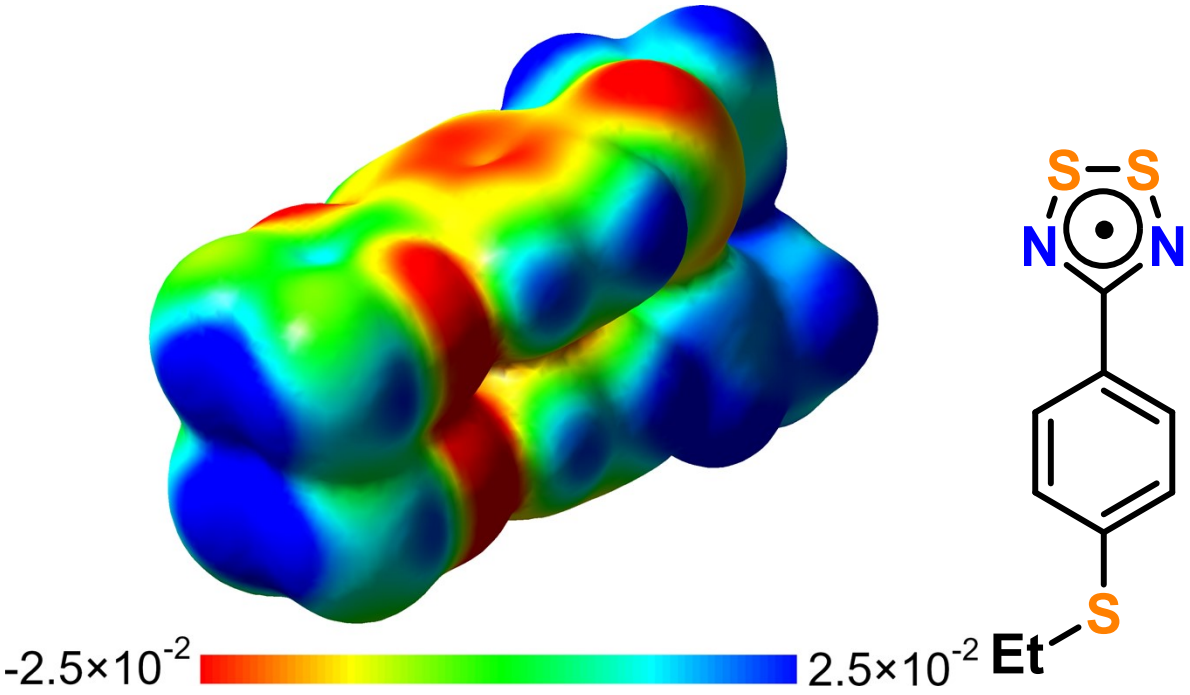

Figure S35. *Electrostatic potential mapped onto the asymmetric unit of* ***3****γ at electron density isovalue of 0.002 atomic units.*

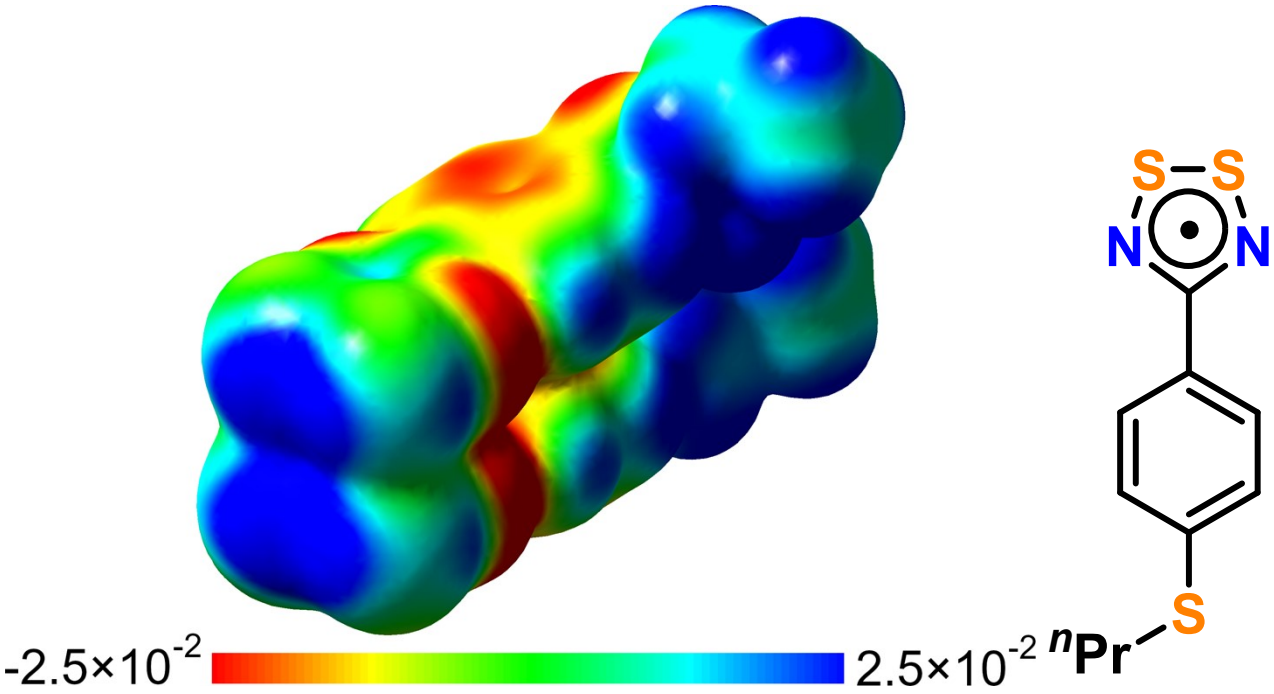

Figure S36. *Electrostatic potential mapped onto the asymmetric unit of* ***4*** *at electron density isovalue of 0.002 atomic units. One of the disordered assemblies was hand-picked.*

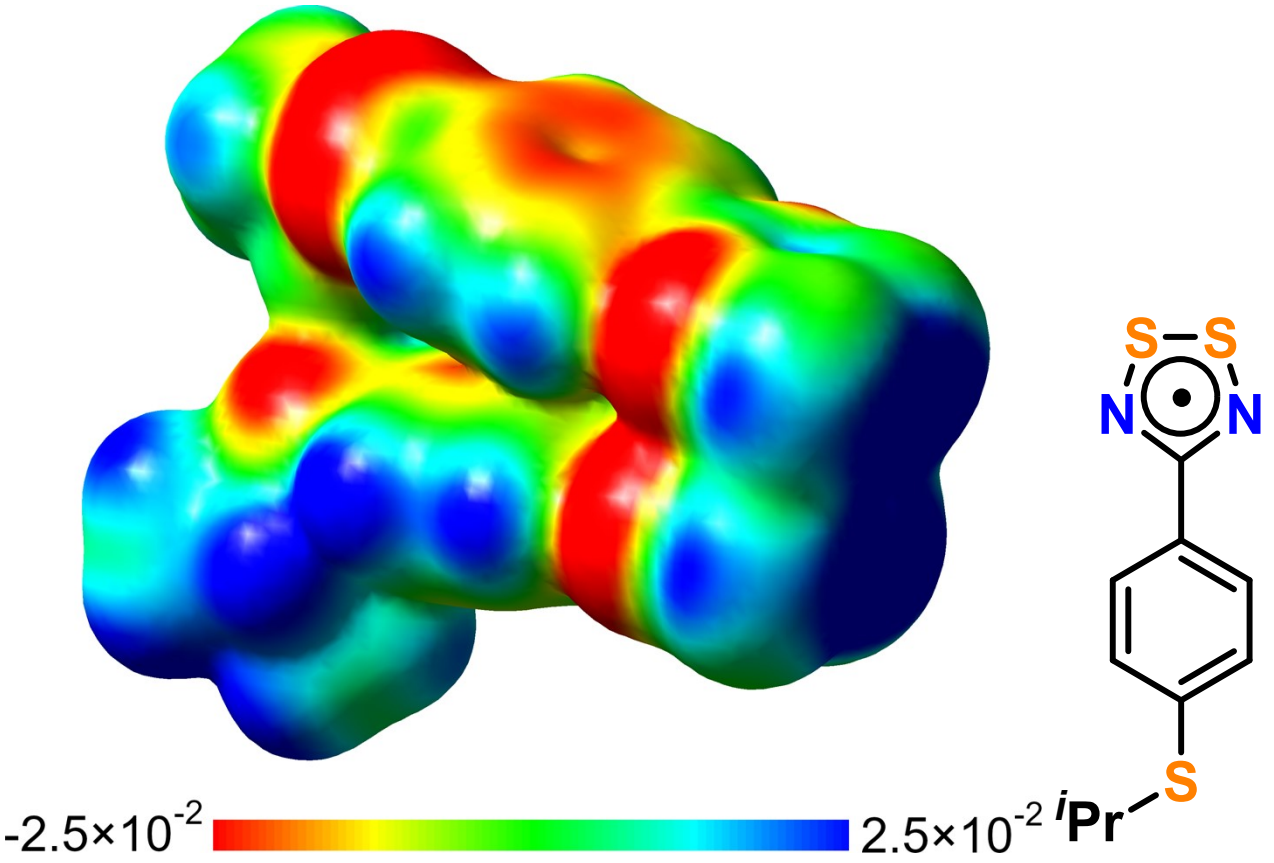

Figure S37. *Electrostatic potential mapped onto the asymmetric unit of* ***5*** *at electron density isovalue of 0.002 atomic units. One of the disordered assemblies was hand-picked.*

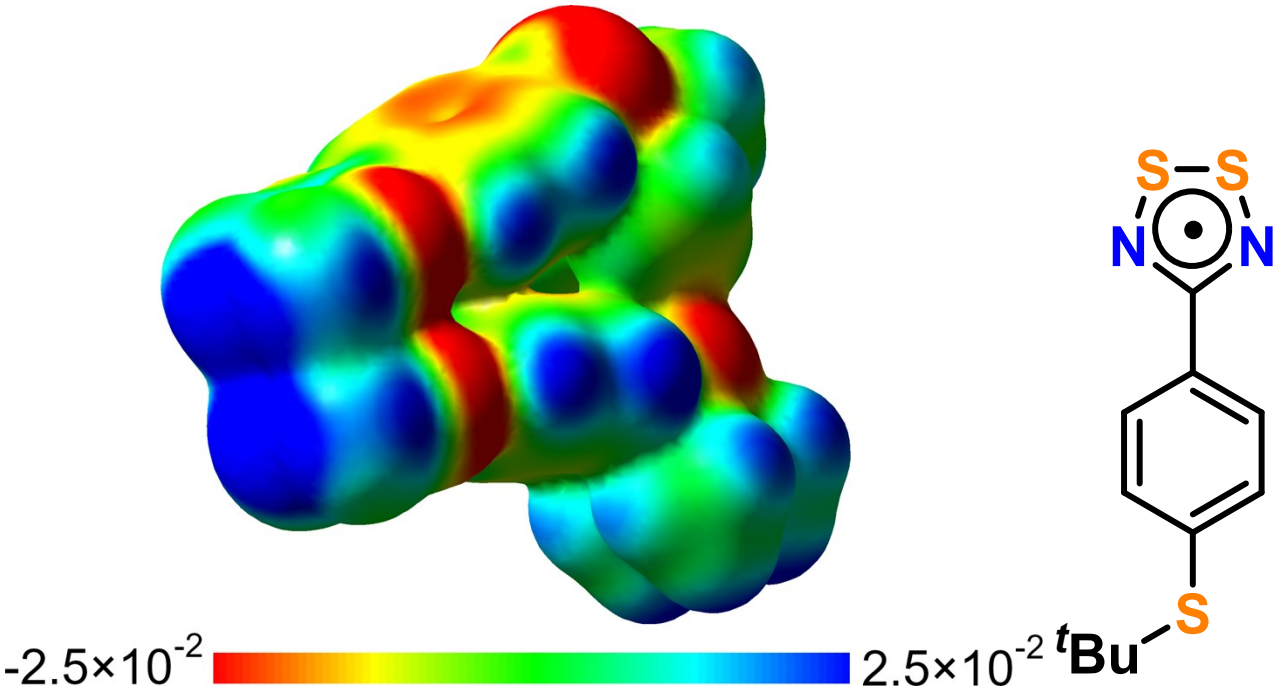

Figure S38. *Electrostatic potential mapped onto the asymmetric unit of* ***6*** *at electron density isovalue of 0.002 atomic units.*

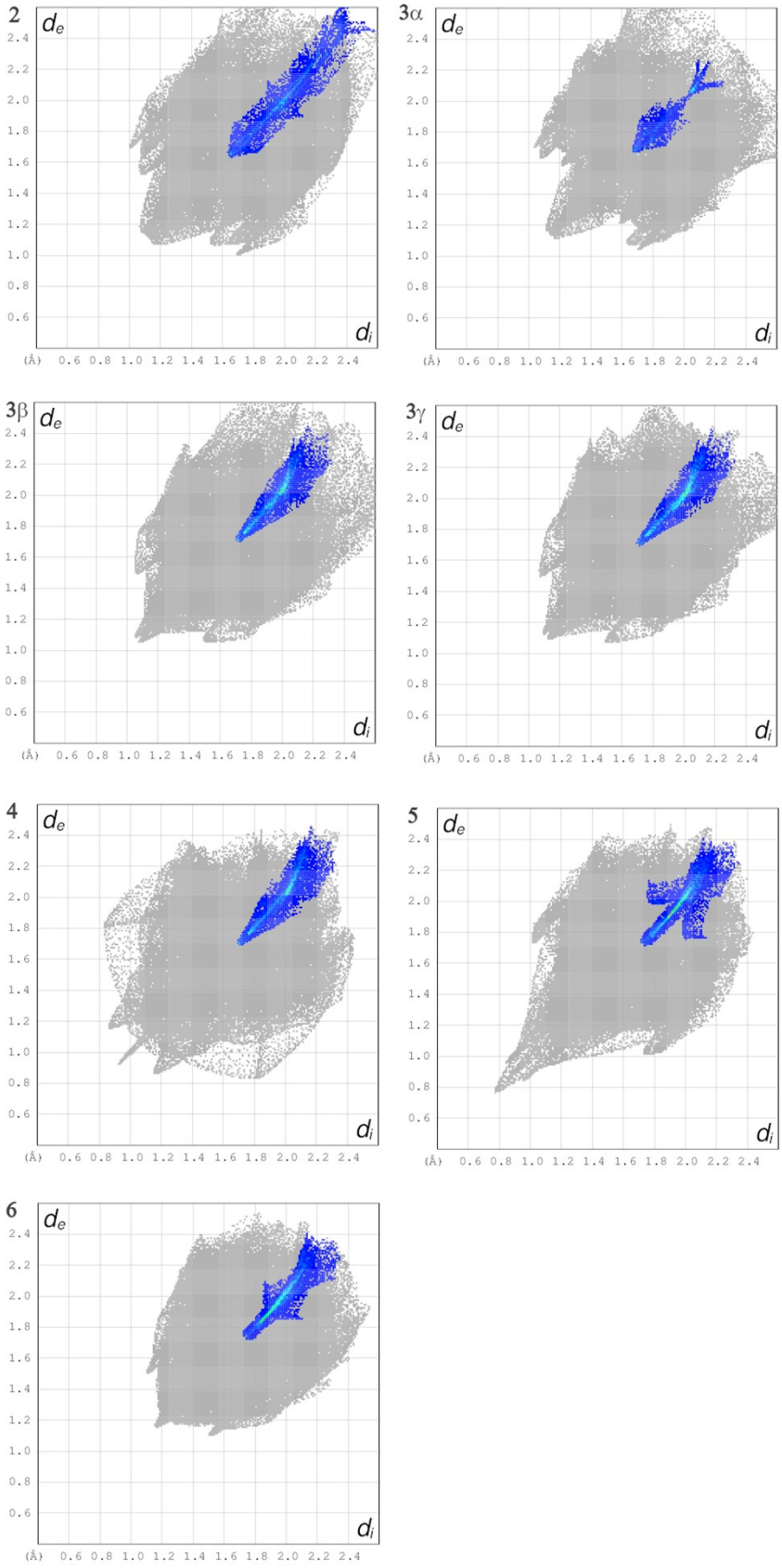

Figure S39. *2D-fingerprints of the Hirshfeld surfaces of* ***1****–****6*** *with highlighted sulfur-sulfur contacts illustrated in blue.*

7 Complete Structural Description of 2 – 6.

Crystal structure of 2 (R = Me). Large, lustrous green blocks of **2** suitable for SCXRD were obtained from the middle zone of a three-zone sublimation (303–323–353 K; See Table S2). The methyl derivative **2** crystallizes in the acentric space group $P2_1$ with *cis*-cofacial π-dimers. The intradimer contacts $d_1 = 3.1496(7)$ and $d_2 = 3.0209(7)$ Å are significantly below the $\sum$vdW = 3.6 Å and are characterized by a hinge angle ($\phi \approx 7.79^\circ$) between the DTDA rings and a near-collinear alignment (torsion angle $\psi \approx 4.5(2)^\circ$) which are comparable to **1** (See Figure 2, S40 and Table 1).

The relatively small steric effect of the MeS-substituents in the dimer affords an S···S' distance ($\Delta = 4.4349(9)$ Å) which is intermediate between the O···O' distances found in the linear-chain, alkoxy-substituted perfluorophenyl derivatives (**M^{R}**, R = Me – Bu).[11] A larger DTDA-phenyl ring twist angle $\theta = 13.2^\circ$ is found in **2** compared to **1** despite the nearly coplanar alignment of the methyl group with the phenyl ring plane, as indicated by the small dihedral angle $\tau \approx 5.1^\circ$. Furthermore, the antiparallel alignment of methyl groups further reduces any steric interaction within the dimer and likely accounts for the similarity between the dimers of **1** and **2**. The average C-S-C bond angle ($\omega \approx 104.05^\circ$) is notably less obtuse than that found for the related C-O-C angle of the alkoxy analogues (**M^{R}**; R = Me − Bu), which range from 118 – 122°, reflecting the reduced s-p hybridization of the sulfur (vs oxygen) in the thioalkyl derivatives.

The solid-state packing in **2** is characterized by short interdimer chalcogen bonding ($d_3 = 3.2912(8)$ and $d_4 = 3.4129(8)$ Å) between the DTDA and alkylthio sulfur atoms. These favorable and directional electrostatic interactions arise from the pronounced σ-hole of the DTDA dimers and a lone pair from the exocyclic sulfur atom of the alkylthio substituent. The combination of the noncovalent chalcogen bonding and the favorable interdimer edge-to-face interactions between the DTDA σ-hole and negative electrostatic potential of the phenyl ring leads to zig-zag chains along the *b*-axis. The combination of these zig-zag chains results in a herringbone arrangement of slipped π-stacks where each dimer is effectively 'sandwiched' between six nearest-neighbor dimers leading to an array of weaker (dispersion, dipole-dipole) intermolecular interactions. The lateral SN-III type interaction between layers arise from the directional interaction of the electronegative DTDA nitrogen and the less pronounced σ-hole along the extension of the S–S bond.

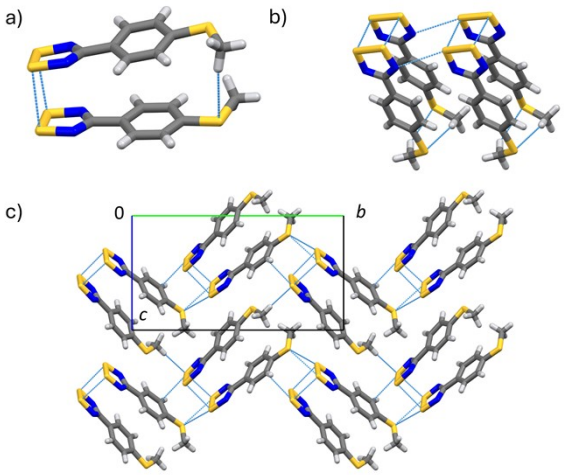

Figure S40. a) The *cis*-cofacial dimers in **2**, b) the SN-type (SN-III) interactions and c) the ABAB herringbone packing with zig-zag chains along the *b* -axis.

Crystal structure of 3α (R = Et). The lustrous green blocks (in reflected light, dark orange in transmitted light) were obtained from MeCN or in the middle sublimation zone (343 K)

and were suitable for SCXRD (See Table S3). The alpha-phase, **3**α crystallizes in the monoclinic space group $P2_1/c$ with *cis*-cofacial π-dimers, as illustrated in Figure 3.. The short intradimer S···S' contacts (d_1 = 3.0908(6) and d_2 = 3.1350(7) Å) are much shorter than the sulfur ∑vdW = 3.6 Å. The near-collinear ($\psi \approx 2.3(1)^\circ$) and essentially coplanar alignment of the DTDA rings (hinge angle $\phi = 4.41^\circ$) is surprising given the gauche conformation of one ethylthio-substituent, which results in its near perpendicular orientation to the phenyl ring plane and a pronounced bowing of one radical of the dimer leading to a large S····S' separation (Δ = 4.7671(7) Å. In contrast, the other ethylthio-group is essentially coplanar with the phenyl ring and the average DTDA-phenyl ring twist angle ($\theta = 9.5^\circ$) in **3**α is like that of **1** ($\theta \approx 8.3^\circ$) despite the apparent increased steric situation created by the different orientation of the EtS-groups. The average C-S-C angles ($\omega \approx 105.06^\circ$) are slightly wider than **2** ($\omega \approx 104.05^\circ$) while the C-C-S-C dihedral angle ($\tau \approx 6.6^\circ$) indicates the methylene (CH_2) carbon of the Et-groups are close to coplanar with the phenyl rings.

The packing motif of **3**α is like **2**, but with slightly longer interdimer chalcogen bonding ($d_3 \approx$ 3.3544(7) and $d_4 \approx$ 3.5211(7) Å) between the DTDA and alkylthio sulfur atoms. This leads to similar zig-zag chains along the *c*-axis and the extreme slippage of the π-stacks leading to a sandwich-like herringbone packing motif where each dimer is surrounded by six nearest-neighbor dimers. The increased slippage induced by the EtS-groups leads to SN-II type lateral interactions (Chart 1) between the DTDA rings as opposed to the SN-III type interactions found in **2**. The combination of these weaker SN-type electrostatic interactions and hydrogen bonding leads to overall weaker interactions along the *b*-axis and appears to be influenced by the orientation and steric effects of the slightly larger EtS-group.

Crystal structure of 3β (R = Et). The small, orange parallelogram-shaped plates of **3**β were isolated directly from the reduction mixture in MeCN and were suitable for SCXRD (See Table S3). Interestingly, **3**β is also the dominant phase (PXRD) obtained by recrystallization of analytically pure **3** from EtCN, by sublimation under static vacuum onto a cold substrate or from melt-recrystallization. The beta-phase crystallizes in the monoclinic space group *P*n with *cis*-cofacial π-dimers, as illustrated in Figure 3. The short intradimer S···S' contacts (d_1 = 3.040(2) and d_2 = 3.085(2) Å; ∑vdW = 3.6 Å) are comparable to those found in **3**γ and **4** (vide infra). The hinge angle in **3**β ($\phi = 5.09^\circ$) is slightly larger than **3**α, and the radicals in **3**β are less collinear ($\psi \approx 6.2(4)^\circ$ vs. 2.3(1)° in **3**α). The average twist angle ($\theta = 7.1^\circ$) in **3**β is comparable to **1** ($\theta \approx 8.3^\circ$) and **4** ($\theta \approx 7.9^\circ$; *vide infra*). In contrast to **3**α, both the EtS-groups are essentially coplanar with the phenyl rings and are antiparallel in the dimers of **3**β, which is evidenced by the smallest dihedral angle $\tau \approx 2.6^\circ$ (See Table 1) and leads to a relatively short S····S' distance (Δ =4.305(2) Å) compared to those found in **1 – 6** (Table 1).

The ABAB herringbone packing motif of **3**β is distinct among the packing of **1 – 6** and leads to short S····S' interdimer interactions (d_3 = 3.505(2) and d_4 = 3.413(2) Å; ∑vdW = 3.6Å) between the orthogonally oriented DTDA rings at the AB π-stack junctions. This arrangement of the dimers into slipped π-stack leads to favorable electrostatic interactions between σ-holes and the electronegative regions above each phenyl ring. This packing motif also leads to the orthogonal orientation of the alkyl groups in the buffering region (Figure 3) and consequently are less interlaced compared to the alkyl chains in **3**γ **– 6**. The hydrogen bonding and SN-III type interactions are optimized by the slight staggering of the π-stacks between layers. Overall, this packing motif maximizes the favorable electrostatic interactions between the DTDA rings and allows van der Waals and dispersion interactions between the alkyl chains but prevents the interaction of the exocyclic sulfur with the DTDA σ-hole as found in **3**α.

Crystal structure of 3γ (R = Et). The small orange plates appear dark green in reflected light but are not as lustrous as **3**α and are obtained from the 303 K sublimation zone or alternatively by recrystallization from EtCN. Despite their smaller size, high-quality, single-crystal X-ray diffraction data was obtained (See Table S3).

The gamma-phase, **3**γ, crystallizes in the monoclinic space group $P2_1/n$ as *cis*-cofacial dimers, as given in Figure 3. As found in all other dimers, the intradimer S···S' contacts (d_1 = 3.075(2) and d_2 = 3.102(2) Å (∑vdW = 3.6 Å) are comparable to **3**α. The hinge angle in **3**γ (ϕ = 5.52°) is slightly larger than on **3**α, and the radicals in **3**γ are less collinear ($\psi \approx 6.3(5)°$ vs. 2.3(1)° in **3**α). The average twist angle (θ = 7.3°) in **3**γ is comparable to **1** ($\theta \approx 8.3°$) and **4** ($\theta \approx 7.9°$; *vide infra*). In contrast to **3**α, both the EtS-groups are essentially coplanar with the phenyl rings in the dimers of **3**γ, which is evidenced by a small dihedral angle $\tau \approx 3.8°$ (See Table 1) and leads to a relatively short S···S' distance (Δ =4.459(3)) compared to found in **1 – 6**. Overall, the dimers metrics of **3**β and **3**γ are very similar but the packing motifs are distinct.

The AA'BB' herringbone packing motif in **3**γ arise from a head-to-head arrangement of the dimers within adjacent π-stacks, which are favoured by the antiperiplanar and antiparallel orientation of the EtS-groups. This effectively buffers the adjacent stacks and leads to mainly weak van der Waals forces and dispersion interactions. As a result, the strongest intermolecular interactions arise at the AB π-stack junctions where short S···S' interdimer interactions (d_3 = 3.518(2) and d_4 = 3.415(2) Å; ∑vdW = 3.6 Å) occur between the DTDA rings. The nearly orthogonal arrangement of the dimers leads to favourable electrostatic interactions between σ-holes and the electronegative regions above each ring, as illustrated in Figure 3.

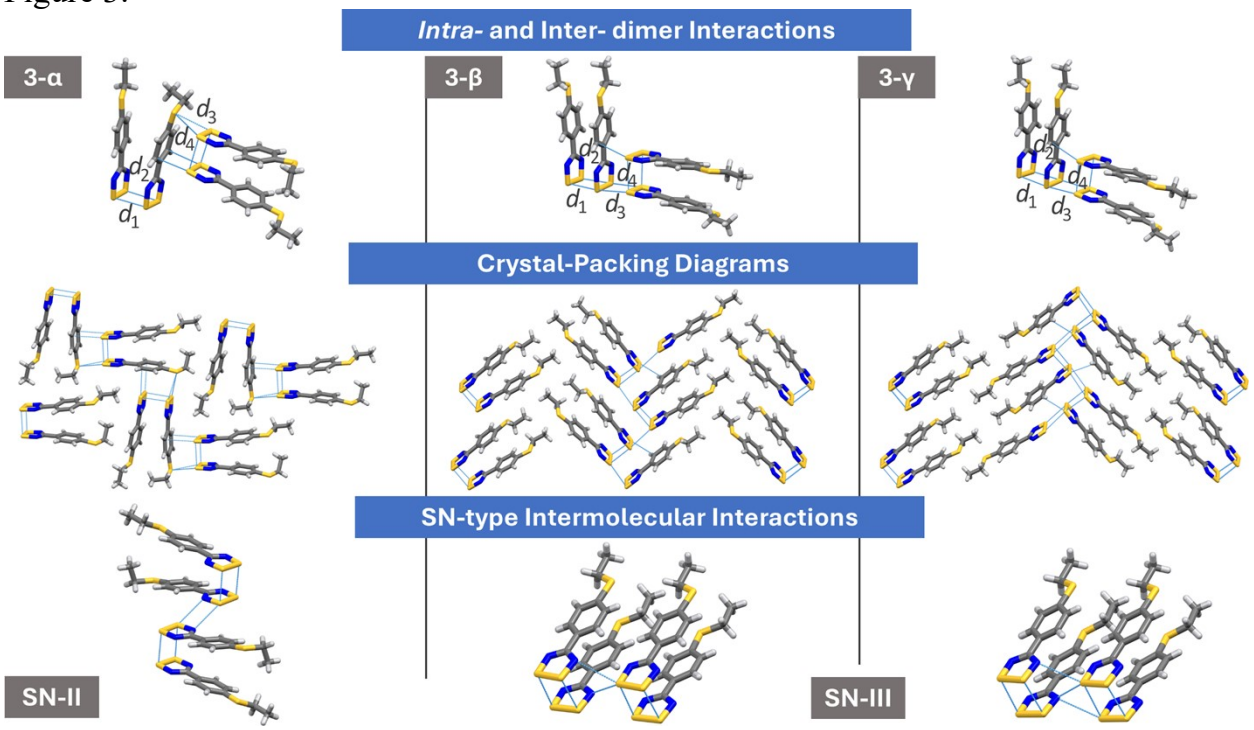

From the main text: Figure 3. Summary of *intra*- and inter-dimer interactions in the three polymorphs of **3** (top), their crystal packing viewed perpendicular to the *ab*-plane (**3**α), or down the *a*-axis (**3**β and **3**γ), and illustrations of the SN-II (**3**α) and SN-III (**3**β and **3**γ) type intermolecular interactions.

Crystal structure of 4 (R = ^{n}Pr). Dark orange plates of **4** suitable for SCXRD were obtained in the middle zone after careful, repeat three-zone temperature gradient sublimation (303–323–343 K, See Table S4). The straight chain, *n*-propylthio-substituted derivative **4**

crystallizes in the monoclinic space group $P2_1/n$ as *cis*-cofacial π-dimers. The intradimer S···S contacts (d_1 = 3.079(1) and d_2 = 3.092(1) Å) are shorter than the ∑vdW = 3.6 Å. The hinge angle (ϕ = 5.61°) in **4** is nearly identical to **3**β, while the torsion ψ = 8.1(2) is slightly larger, likely due to the gauche orientation of the *n*-propyl groups, which is like in **3**α. The ^{n}Pr-groups are disordered therefore the metrical parameters are based on the dominant component of the disorder model (minor component only influences τ slightly while ω is relatively unchanged). Despite the presence of the longer and slightly bulkier alkyl chain in **4** the average twist angle (θ = 7.9°) is most comparable to **1** ($\phi \approx 8.3°$) while the C-S-C angle ($\omega \approx 104.45°$) and the C-C-S-C dihedral angle ($\tau \approx 6.4°$) are comparable to those found in **2**, **3**α and **3**β but the S···S' distance Δ = 4.510(4) Å is slightly longer because the torsion angle in **4** is the largest found in **1–6**.

The AA'BB' herringbone packing motif in **4**, when viewed down the *a*-axis, appears surprisingly like **3**γ despite the disordered and differently oriented ^{n}Pr groups. The short interdimer S···S' contacts ($d_3 \approx 3.546(1)$ and $d_4 \approx 3.413(1)$ Å; ∑vdW = 3.6 Å.) between the DTDA rings are nearly identical to **3**β. Similarly, these short S···S' contacts favor the interaction of the electropositive DTDA σ-hole and the electronegative regions of the DTDA and phenyl rings. The ^{n}Pr groups which provide a similar buffering effect between the head-to-head arrangement of π-stack dimers as found in **3**β (vide supra), however, one propyl group is roughly antiperiplanar while the other adopts a gauche-like conformation. This helps to minimize steric clashes between the alkyl groups within the dimers, but it appears that this leads to lesser interdigitation of the propyl-chains within the AA or BB π-stacks. This likely explains the divergent thermal behavior (early onset of melting and sublimation) found for **3**β and **4** and discussed in more detail in the main text.

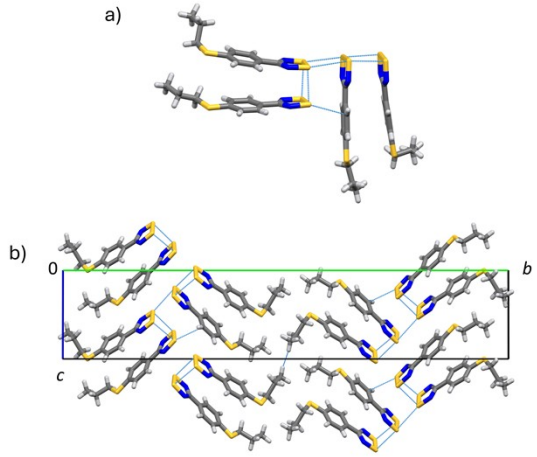

Figure S41. a) The *cis*-cofacial dimers in **4** and their orthogonal alignment b) the AA'BB' herringbone packing viewed down the *a*-axis.

Crystal structure of 5 (R = ^{i}Pr). Needle-like crystals of **5** suitable for SCXRD were obtained in the middle zone after careful, repeated three-zone temperature gradient sublimation (313–323–353 K, see Table S4). The branched, isopropyl derivative **5** crystallizes in the monoclinic space group $P2_1/c$, as *cis*-cofacial π-dimers. The intradimer S···S contacts (d_1 = 3.079(1) and d_2 = 3.076(1) Å; ∑vdW = 3.6 Å) are comparable to those found in **1 – 6**. The hinge angle (ϕ = 6.44°) between the DTDA ring planes is relatively small and like that found in **1**, **2** and **3**α, suggesting the rings are essentially coplanar, while the torsion angle ($\psi \approx 0.4(2)°$) is negligible, indicating the radicals in the dimers are essentially collinear. The relatively large S···S' distance (Δ = 5.168(2) Å) is like in **3**α (Table 1), but significantly longer than on **2**, **3**β, and **4**. Likewise, the average twist angle (θ = 10.1°) and C-S-C angle ($\omega \approx 106.56°$) in **5** are relatively

large, and together with the pronounced bowing of one radical in the dimer suggests the isopropyl group has significant steric influence in this system. Not surprisingly, the average C-C-S-C dihedral angle ($\tau \approx 62.5^{\circ}$) is much larger than in the unbranched, straight-chain alkyl derivatives indicating the ^{i}Pr-group deviates more sharply from the near coplanarity more commonly found in **2**, **3** and **4**. Predictably, there is also some disorder among the isopropyl groups given its rotational degrees of freedom, however, the conformational flexibility may be limited by steric hinderance, which appears to constrain the position of the ^{i}Pr-group in the solid-state. This leads to equal components and the metrical parameters given represent the average positional disorder, unless otherwise stated.

Radical **5** maintains the AA'BB' herringbone packing motif with short interdimer S···S' contacts (d_3 = 3.5479(9) and d_4 = 3.4466(9) Å) between the DTDA rings on adjacent dimers are less than the ∑vdW = 3.6Å and align with the **1 – 6** series (Table 1) suggesting the conserved σ-hole-driven packing. While the alkyl groups in **3**β and **4** buffer the herringbone π-stacks into stratified layers along the *a*-axis, the isopropyl groups in **5** disrupt this ordering. Instead, they adopt zig-zag topology when viewed in the [204] lattice plane, as illustrated in Figure 5d. These chains are stabilized by weak dispersion interactions between interlaced *i*Pr-groups, while the branched substituents introduce additional interchain CH–π, hydrogen-bonding, and SN-III type (Chart 1) interactions, which may affect the thermal stability of **5**. The loss of layer stratification contrasts with **1 – 4** highlighting how the steric demand of the *i*Pr ($\tau \approx 62.5^{\circ}$ vs. $\tau \leq 7^{\circ}$ in **2 – 4**) modulates the supramolecular hierarchy in **5**.

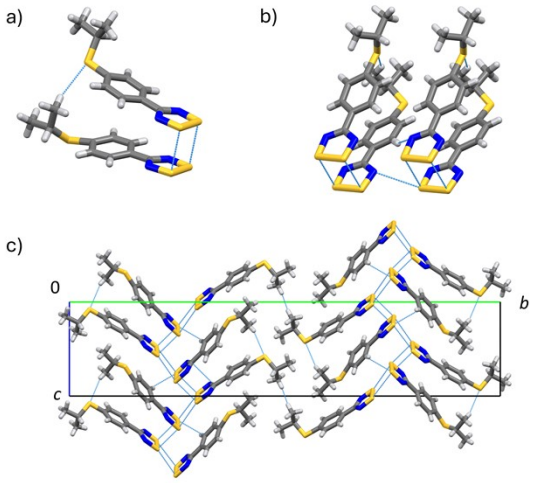

Figure S42. a) The *cis*-cofacial dimers in **5**, b) the SN-type (SN-III) interactions and c) the AA'BB' herringbone packing viewed down the *a*-axis.

Crystal structure of 6 (R = ^{t}Bu). Single crystals of **6** suitable for SCXRD were obtained by three-zone gradient vacuum sublimation (303–333–353 K, See Table S4). The structure crystallizes in the monoclinic space group $P2_1/n$ forming *cis*-cofacial dimers. The intradimer S···S contacts (d_1 = 3.063(1) and d_2 = 3.086(1) Å) are significantly shorter than the ∑vdW = 3.6Å. The geometrical parameters in **6** are like **2** (hinge angle ϕ = 8.32° vs. 7.79° in **2**; average twist angle θ = 11.6° vs 13.2° in **2;** Table 1), however, there are notable distortions. The near orthogonal C-C-S-C dihedral angle ($\tau \approx 89.7^{\circ}$) and minimal torsion angle ($\psi \approx 1.4(2)^{\circ}$) impact the dimer geometry most significantly. This results in severe eclipses of the ^{t}Bu-groups (unique in this series), and to a pronounced bowing of one radical in the dimer. It is surprising the ^{t}Bu-groups do not adopt an antiparallel arrangement as in **2** and **3**β to relieve strain within the dimer but the more acute C-S-C bond angle ($\omega \approx 103.25^{\circ}$) and steric bulk of the ^{t}Bu-group

appear to prevent such a conformation. The structure appears to be stabilized by favorable CH···S hydrogen bonding between the ^{t}Bu methyl groups and exocyclic sulfurs and bowing-induced relief of phenyl ring electrostatic repulsion. The well-defined positions of the ^{t}Bu-groups in **6** contrasts sharply with the rotational disorder observed for smaller alkyl chains in **4 – 5**, demonstrating how steric bulk restricts molecular flexibility and suppresses dynamic disorder in crystalline state. While maintaining the AA'BB' herringbone packing seen in **3**γ **– 5**, compound **6** exhibits conserved σ-hole-driven packing through with short interdimer S···S' contacts ($d_3 \approx 3.476(1)$ and $d_4 \approx 3.613(1)$ Å) less than the ∑vdW = 3.6Å. Notably, the steric demand of the ^{t}Bu-group induces pronounced slippage of the π-stacks leading to an unusual S···π interaction between exocyclic sulfur and the DTDA ring. A zig-zag chain motif in the [204] plane (*cf.* **5**), where staggered alignment minimizes the interchain contacts and eliminates any significant S···N chalcogen bonding (Chart 1; ΣvdW = 3.2 Å) between chains.

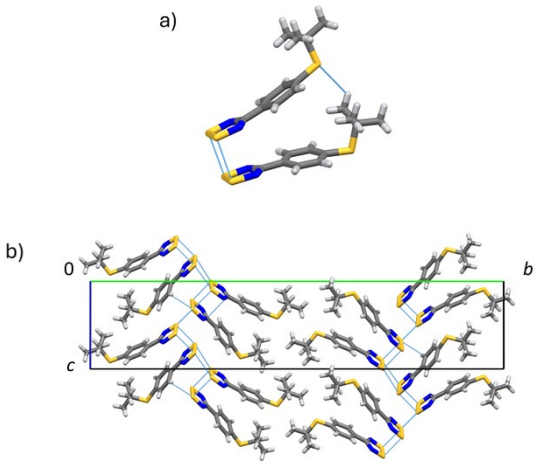

Figure S43. a) The *cis*-cofacial dimers in **6** and b) the AA'BB' herringbone packing viewed down the *b*-axis.

8 References

(1) Chiu, H.-C.; Pearce, A. J.; Dunn, P. L.; Cramer, C. J.; Tonks, I. A. β-Oxo-δ-Diimine Nickel Complexes: A Comparison of Tautomeric Active Species in Ethylene Polymerization Catalysis. *Organometallics* **2016**, *35* (12), 2076–2085. https://doi.org/10.1021/acs.organomet.6b00256.

(2) Fulmer, G. R.; Miller, A. J. M.; Sherden, N. H.; Gottlieb, H. E.; Nudelman, A.; Stoltz, B. M.; Bercaw, J. E.; Goldberg, K. I. NMR Chemical Shifts of Trace Impurities: Common Laboratory Solvents, Organics, and Gases in Deuterated Solvents Relevant to the

Organometallic Chemist. *Organometallics* **2010**, *29* (9), 2176–2179. https://doi.org/10.1021/om100106e.

(3) *CrysAlis Pro | Rigaku Global Website*. https://www.rigaku.com/products/crystallography/crysalis#app (accessed 2022-09-14).

(4) Sheldrick, G. M. SHELXT – Integrated Space-Group and Crystal-Structure Determination. *Acta Crystallogr. Sect. Found. Adv.* **2015**, *71* (1), 3–8. https://doi.org/10.1107/S2053273314026370.

(5) Sheldrick, G. M. Crystal Structure Refinement with SHELXL. *Acta Crystallogr. Sect. C Struct. Chem.* **2015**, *71* (1), 3–8. https://doi.org/10.1107/S2053229614024218.

(6) Gruene, T.; Hahn, H. W.; Luebben, A. V.; Meilleur, F.; Sheldrick, G. M. Refinement of Macromolecular Structures against Neutron Data with SHELXL2013. *J. Appl. Crystallogr.* **2014**, *47* (1), 462–466. https://doi.org/10.1107/S1600576713027659.

(7) Dolomanov, O. V.; Bourhis, L. J.; Gildea, R. J.; Howard, J. a. K.; Puschmann, H. OLEX2: A Complete Structure Solution, Refinement and Analysis Program. *J. Appl. Crystallogr.* **2009**, *42* (2), 339–341. https://doi.org/10.1107/S0021889808042726.

(8) Frisch, M. J.; Trucks, G. W.; Schlegel, H. B.; Scuseria, G. E.; Robb, M. A.; Cheeseman, J. R.; Scalmani, G.; Barone, V.; Petersson, G. A.; Nakatsuji, H.; Li, X.; Caricato, M.; Marenich, A. V.; Bloino, J.; Janesko, B. G.; Gomperts, R.; Mennucci, B.; Hratchian, H. P.; Ortiz, J. V.; Izmaylov, A. F.; Sonnenberg, J. L.; Williams; Ding, F.; Lipparini, F.; Egidi, F.; Goings, J.; Peng, B.; Petrone, A.; Henderson, T.; Ranasinghe, D.; Zakrzewski, V. G.; Gao, J.; Rega, N.; Zheng, G.; Liang, W.; Hada, M.; Ehara, M.; Toyota, K.; Fukuda, R.; Hasegawa, J.; Ishida, M.; Nakajima, T.; Honda, Y.; Kitao, O.; Nakai, H.; Vreven, T.; Throssell, K.; Montgomery Jr., J. A.; Peralta, J. E.; Ogliaro, F.; Bearpark, M. J.; Heyd, J. J.; Brothers, E. N.; Kudin, K. N.; Staroverov, V. N.; Keith, T. A.; Kobayashi, R.; Normand, J.; Raghavachari, K.; Rendell,

A. P.; Burant, J. C.; Iyengar, S. S.; Tomasi, J.; Cossi, M.; Millam, J. M.; Klene, M.; Adamo, C.; Cammi, R.; Ochterski, J. W.; Martin, R. L.; Morokuma, K.; Farkas, O.; Foresman, J. B.; Fox, D. J. Gaussian 16 Rev. C.01, 2016.

(9) Weigend, F.; Ahlrichs, R. Balanced Basis Sets of Split Valence, Triple Zeta Valence and Quadruple Zeta Valence Quality for H to Rn: Design and Assessment of Accuracy. *Phys. Chem. Chem. Phys.* **2005**, *7* (18), 3297–3305. https://doi.org/10.1039/B508541A.

(10) Adamo, C.; Barone, V. Toward Reliable Density Functional Methods without Adjustable Parameters: The PBE0 Model. *J. Chem. Phys.* **1999**, *110* (13), 6158–6170. https://doi.org/10.1063/1.478522.

(11) Spackman, M. A.; Jayatilaka, D. Hirshfeld Surface Analysis. *CrystEngComm* **2009**, *11* (1), 19–32. https://doi.org/10.1039/B818330A.

(12) Spackman, P. R.; Turner, M. J.; McKinnon, J. J.; Wolff, S. K.; Grimwood, D. J.; Jayatilaka, D.; Spackman, M. A. CrystalExplorer: A Program for Hirshfeld Surface Analysis, Visualization and Quantitative Analysis of Molecular Crystals. *J. Appl. Crystallogr.* **2021**, *54* (3), 1006–1011. https://doi.org/10.1107/S1600576721002910.